REPORT

BRAIN RESEARCH

Vectorial representation of spatial goals in the hippocampus of bats

Ayelet Sarel,* Arseny Finkelstein,*† Liora Las, Nachum Ulanovsky‡

To navigate, animals need to represent not only their own position and orientation, but also the location of their goal. Neural representations of an animal's own position and orientation have been extensively studied. However, it is unknown how navigational goals are encoded in the brain. We recorded from hippocampal CA1 neurons of bats flying in complex trajectories toward a spatial goal. We discovered a subpopulation of neurons with angular tuning to the goal direction. Many of these neurons were tuned to an occluded goal, suggesting that goal-direction representation is memory-based. We also found cells that encoded the distance to the goal, often in conjunction with goal direction. The goal-direction and goal-distance signals make up a vectorial representation of spatial goals, suggesting a previously unrecognized neuronal mechanism for goal-directed navigation.

Navigation, the ability to reach a desired goal location, is essential for humans and animals. Decades of research have focused on the neural representation of an animal's own location and orientation, revealing the existence of place cells (*1*–*3*), grid cells (*4*, *5*), and head-direction cells (*6*, *7*). However, a fundamental question that remains unanswered is how an animal's spatial goals are encoded in the brain. One suggested mechanism posits that the goal is represented by activating a sequence of place cells from the animal's current location to the goal location (*8*, *9*). An alternative mechanism would be to rely on a vectorial representation of the goal—i.e., encoding the direction and distance to the goal. This mechanism has been suggested both theoretically (*10*–*13*) and by behavioral studies in a variety of species (*14*–*19*); however, a representation of such vectors in the brain has not been found to date.

We trained Egyptian fruit bats to fly in highly complex trajectories within a large flight room and land on a single landing site, defined as the goal, where the bat could eat and rest (Fig. 1A and fig. S1). We computed the egocentric azimuthal goal-direction angle, defined as the heading direction of the bat with respect to the goal (Fig. 1B) (we focused all our analyses on the two-dimensional horizontal projection, because the bats' behavior was mostly confined to a narrow horizontal slab around the z height of the goal; fig. S2). While the bats performed this goal-directed task and sampled all goal-direction angles (Fig. 1C), we recorded the activity of 309 single neurons from hippocampal area CA1 of three bats (Fig. 1D), using a wireless electrophysiology device (*20*). A subpopulation of hippocampal neurons exhibited angular tuning to the egocentric goal direction [Fig. 1, E (three leftmost examples, top row) and F]. We classified 19% of the CA1 neurons (58 of 309) as significant goal-direction cells on the basis of tuning directionality (95th percentile in a shuffling analysis), tuning stability, and tuning reconstruction analysis (*20*, *21*). The distribution of preferred goal-direction angles across these cells spanned the entire 360° range (Fig. 1, F and G) but exhibited overrepresentation of preferred goal-direction angle 0° (Fig. 1, F and G; see also Fig. 1E, cells 213 and 287)—i.e., a substantial fraction of cells fired maximally when the bat was heading toward the goal.

Of the 58 goal-direction cells, 26 neurons (45%) exhibited angular tuning to the goal with no significant place tuning (e.g., Fig. 1E, cell 213), whereas 32 neurons (55%) showed both goal-direction tuning and place tuning (e.g., Fig. 1E, cells 287 and 131; summary in Fig. 1H). We also found 101 classical place cells, making up 33% of the recorded CA1 neurons, a similar fraction to that found in previous studies of place cells in rats and bats (*2*, *3*). Most of the place cells (69 cells, 68%) had no goal-direction tuning (e.g., Fig. 1E, cell 77; Fig. 1H), consistent with the classical hippocampal place code.

To verify that the goal-direction signal is genuine and not biased by the place tuning, we did the following. First, one of our inclusion criteria for goal-direction cells required the neuron to have stronger goal-direction tuning than place tuning, based on a reconstruction analysis, yielding a goal/place index > 1 (Fig. 1I and fig. S3) (*20*). This very strict criterion ensured that the goal-direction tuning of all the neurons that we studied could not be explained through coupling of pure place tuning and the bat's behavior ($P < 2 \times 10^{-4}$ for all of the 58 goal-direction cells; Fig. 1I and fig. S3). Second, almost half of the goal-direction cells were not significantly place-tuned (e.g., Fig. 1E, cell 213; Fig. 1H; $n = 26$). Third, for cells that were tuned to goal direction and place, the firing within the place field was highly reduced when the bat was flying in the null direction (180° from the preferred goal direction) (fig. S4). Fourth, we computed the goal-direction tuning separately inside and outside the place field (Fig. 1J) (*20*). Many of the goal-direction cells exhibited similar preferred goal directions inside and outside the place field (Fig. 1, J and K). Next, we repeated the same types of analyses to dissociate between the goal-direction signal and the head-direction signal reported in the hippocampus (*21*, *22*); we found that the goal-direction signal was largely independent of the head-direction signal (fig. S5). Furthermore, 31% of the goal-direction cells (18 of 58) were significantly tuned only to goal direction but not to head direction or to place.

The neurons stably maintained their goal-direction tuning throughout the flight to the goal [Fig. 1, L and M (left panel)], including well before landing, despite the fact that the bats' flights were long and complex and spanned highly variable angles (Fig. 1, A and C, and fig. S1). The goal-direction tuning was also stable along the entire behavioral session [Fig. 1, E (three leftmost examples; note the stable raster of spikes along the session) and M (right)]. To verify that the tuning was specific to the goal, we computed the tuning to every location (every pixel) in the room as though it was a goal. The goal-direction cells were sharply tuned to the true goal, but not to other locations in the environment (fig. S6).

During real-life navigation, the goal could be invisible to the animal, meaning that goal-directed navigation requires memory (*23*). We therefore conducted another session at the beginning of every recording day, in which we occluded the goal by an opaque curtain that blocked vision, echolocation, and olfaction (Fig. 2A, top). This hidden-goal session was conducted with two of the three bats ($n = 158$ recorded cells). Tuning to the hidden goal was computed using only epochs when bats could not see the goal. A substantial fraction of cells (43 of 158, or 27%) exhibited significant directional tuning to the hidden goal [Fig. 2B (examples, top row) and fig. S7]. These cells were tuned significantly more sharply to the hidden goal than to the curtain edges, as quantified by comparing the directionality index [the Rayleigh vector length (*20*); fig. S8, A to C; t test, $P < 0.03$]. The goal-direction tuning was invariant to flight trajectory—i.e., the tuning did not change if the bat eventually flew to the hidden goal from the left or right side of the curtain (fig. S8, E to H)—suggesting trajectory-invariant representation of hidden goals "through the wall."

We next examined the effect of changing the goal location. In the second session of the curtain experiment, we moved the goal to the center of the room (Fig. 2A, bottom) (i.e., the original experiment shown in Fig. 1A). Of 43 cells tuned to the hidden goal, 27 (63%) lost this tuning when the goal was not there anymore (Fig. 2B, three leftmost examples, bottom row; cell 207 exemplifies the 37% of neurons that did not lose

Department of Neurobiology, Weizmann Institute of Science, Rehovot 76100, Israel.
*These authors contributed equally to this work. †Present address: Janelia Research Campus, Howard Hughes Medical Institute, Ashburn, VA 20147, USA. ‡Corresponding author. Email: nachum.ulanovsky@weizmann.ac.il

Downloaded from http://science.sciencemag.org/ on January 24, 2017

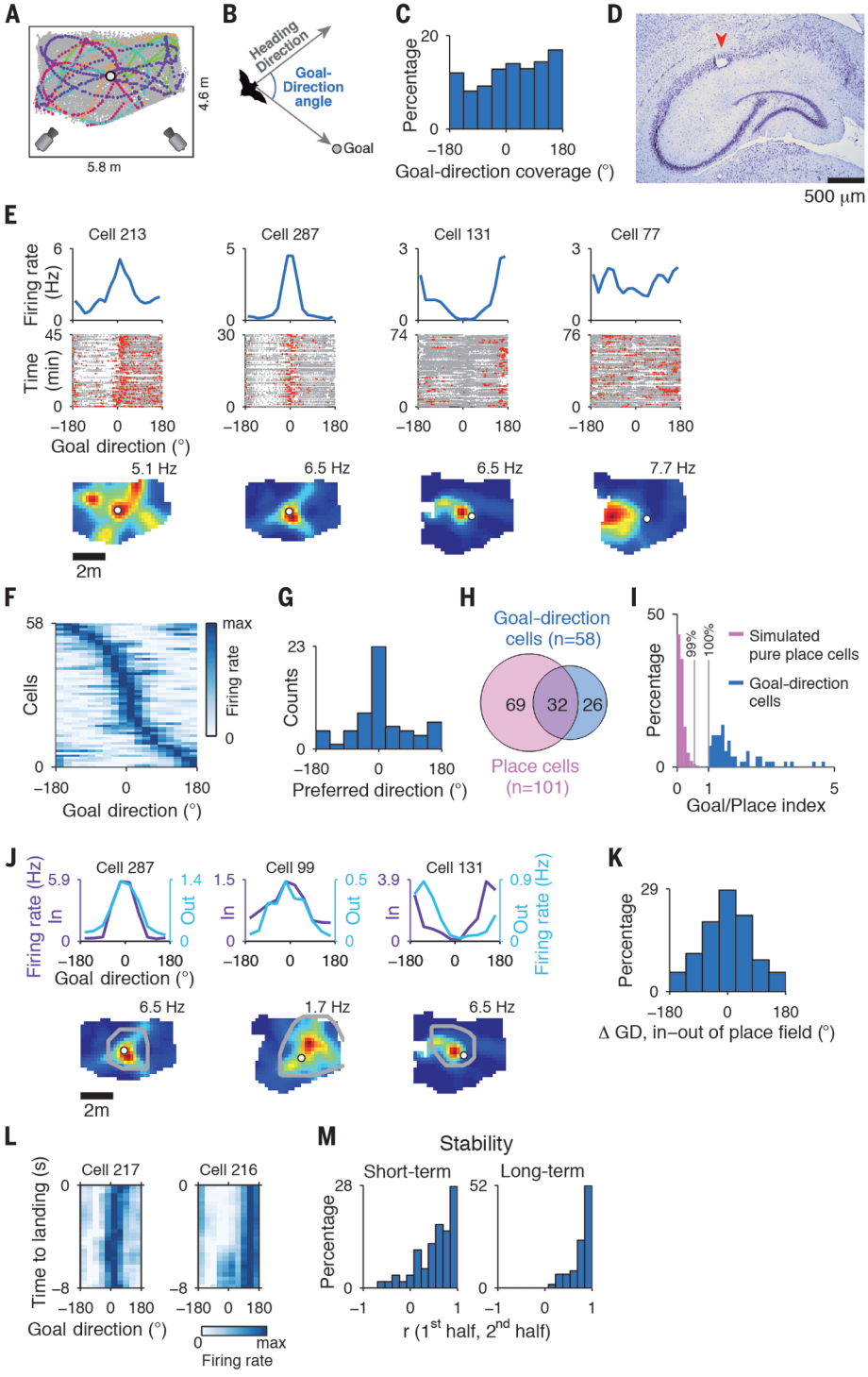

Fig. 1. Goal-direction tuning in bat hippocampal area CA1. (**A**) Behavioral setup, showing the flight room (5.8 by 4.6 by 2.7 m; top view) with one elevated landing point (the goal; circle). Five flight trajectories are highlighted in different colors on top of the behavioral coverage for that day (gray). Cameras are shown in the lower corners. (**B**) Goal-direction angle (blue), defined as the azimuthal angle between the heading direction (top arrow) and the bat-to-goal direction (bottom arrow). (**C**) Distribution of time spent by all bats in different goal-direction angles. (**D**) Coronal section through the dorsal hippocampus of one of the bats. Arrowhead, lesion at end of the tetrode track. (**E**) Four example cells (columns). Top, goal-direction tuning curves. Middle, goal-direction angles along the behavioral session (gray), with spikes overlaid (red). Bottom, spatial firing-rate maps [top view; color scale, zero (blue) to maximal firing rate (red, value indicated)]. Cell 213, goal-direction cell without place tuning; cells 287 and 131, tuned to both goal direction and place; cell 77, pure (classical) place cell. (**F**) Normalized goal-direction tuning for all significant goal-direction cells (n = 58; rows, sorted by preferred direction). (**G**) Distribution of preferred goal directions. (**H**) Total numbers of recorded goal-direction and place cells in CA1. (**I**) Distribution of the goal/place index for all goal-direction cells (blue; n = 58) and for simulated pure place cells (pink; n = 5625). Goal-direction tuning could not be explained by pure place tuning ($P < 2 \times 10^{-4}$ for all 58 goal-direction cells; vertical lines, 99th and 100th percentile for the simulated cells). (**J**) Examples of in-field/out-of-field analysis for three cells (columns). Top, goal-direction tuning curves for in-field (dark purple) and out-of-field (light blue) data. Bottom, firing-rate maps (top view; gray line, in-field area). (**K**) Distribution of differences in preferred goal direction (ΔGD) between in-field and out-of-field tuning curves. (**L**) Two example cells, showing the normalized goal-direction tuning curves (rows) for different times along the complex flights. (**M**) Stability of goal-direction tuning (n = 58 goal-direction cells). Shown are correlations of tuning curves between the first and second halves of the flight (short-term stability, left) and between the first and second halves of the behavioral session (long-term stability, right).

their tuning). Similarly, 21 (68%) of the 31 cells that were tuned to the centrally located goal in the second session were untuned when the goal was not there (Fig. 2C). These extreme changes in tuning (Fig. 2, B and C) could not be explained by behavioral changes between the sessions, recording instability, or selection bias (fig. S9). For a subset of neurons, we recorded three sessions (hidden goal → central goal → hidden goal) and found that the goal-direction tuning was conserved across the two hidden-goal sessions (Fig. 2D; compare sessions 1 and 3). Among the population of goal-direction neurons recorded in the curtain experiments, most cells were significantly more tuned to the goal than to the same spatial position when the goal was not there—as was quantified by a change in the tuning modulation depth index (*20*) (Fig. 2E; t test for cells tuned to the hidden goal, $P < 10^{-5}$; t test for cells tuned to the central goal, $P < 0.005$)—suggesting that the tuning is indeed goal-related. Further, the majority of goal-direction cells (60 of 74, or 81%) were significantly tuned to only one of the two goals, either the hidden goal in session 1 or the central goal in session 2, indicating that the goal-direction tuning is largely goal-specific.

To examine the tuning changes between the sessions at better temporal resolution, we computed the goal-direction tuning over the course of the sessions in short time bins (Fig. 2, F and G). Some of the cells abruptly changed their tuning when the goal moved to the new location (Fig. 2F). A handful of cells that were tuned to the hidden

Downloaded from http://science.sciencemag.org/ on January 24, 2017

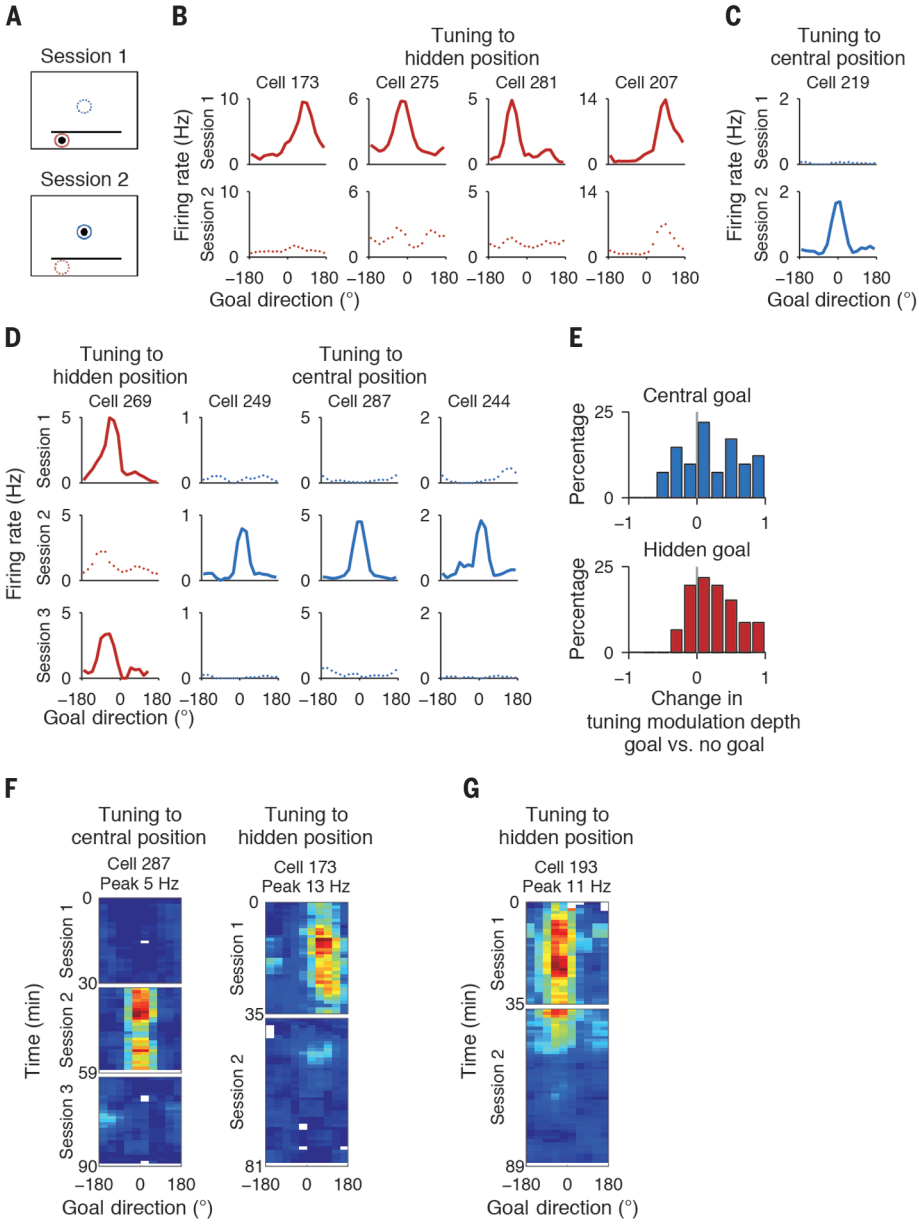

Fig. 2. Goal-direction tuning is memory-based. (**A**) Behavioral setups (top view) for two consecutive sessions. In each session, there was only one goal (black filled circle), located either behind an opaque curtain (top, session 1, hidden goal session) or at the center of the room (bottom, session 2, central goal session). Black horizontal line, curtain position (fixed across sessions and days). Blue and red circles, positions for which we computed the tuning curves in (B) to (D); dotted circles are empty locations (no goal). In this experiment, we recorded 158 cells from two bats. (**B** to **D**) Examples of goal-direction cells (columns) for different sessions (rows). Red and blue tuning curves were computed for the red and blue circles in (A). Dotted tuning curves [computed for dotted circles in (A)] indicate tuning to empty locations. All tuning curves were computed on the basis of epochs when the bat could not see the hidden goal. Four examples of cells tuned to the hidden goal in session 1 are shown in (B); the three leftmost cells lost their tuning in session 2. Shown in (C) is an example of a neuron tuned to the central goal only in session 2. Examples of goal-direction cells recorded for three sessions (hidden session → central session → hidden session) are shown in (D). Cell 269 was tuned to the hidden goal in sessions 1 and 3; the other examples (blue) were tuned to the central goal only in session 2. (**E**) Distributions of changes in tuning modulation depth, comparing the tuning to the same location with versus without a goal. Top, cells tuned to the central goal ($n = 31$); bottom, cells tuned to the hidden goal ($n = 43$). The tuning changes were highly significant (t test; top, $P < 0.005$; bottom, $P < 10^{-5}$). (**F** and **G**) Three example neurons, showing the dynamics of goal-direction tuning over the sessions. Colors are scaled for each neuron, from zero (blue) to the maximal firing rate across all sessions (red, value indicated). Two neurons that changed their tuning abruptly at the transition point between sessions are shown in (F). Shown in (G) is a neuron that was tuned to the hidden goal in the first session and exhibited a gradual decay in its tuning when the goal was moved.

goal in the first session showed a slow decay in the tuning over the ~10 to 15 min after we moved the goal, which might indicate a memory trace for the previous goal location (Fig. 2G).

In addition to knowing the goal direction, it could be useful for the animal to know the distance to the goal. Sixteen percent of the CA1 neurons (49 of 309) were modulated by the path distance to the goal (Fig. 3, A and B, and fig. S10) (*20*). Most of these goal-distance cells fired maximally at short path distances of between 0 and −2 m, i.e., when the bat was approaching the goal [Fig. 3, A (four leftmost examples) and B]. These neurons could be interpreted as signaling the expectation of imminent reward, which is difficult to disentangle experimentally from coding of distance to goal per se, because for a flying bat, it is always rewarding to land on a goal to rest. However, almost half of the cells fired well before landing on the goal and had preferred path distances of <−2 m, and for some cells even as far as −10 m [Fig. 3, A (two rightmost examples) and B, and fig. S10 (right)]—suggesting that, at least for these neurons, the distance tuning did not reflect the bat's expectation of reward.

We next examined the relation between distance tuning and goal-direction tuning and found a significant correlation between the two: Neurons that were more strongly tuned to path distance were also more strongly tuned to goal direction [Fig. 3C; Pearson correlation between directionality index and path-distance index (*20*), $r = 0.65$, $P < 10^{-6}$]. This suggested a conjunctive representation of goal direction and distance, which was indeed substantiated by plotting the goal-direction tuning for different distances to the goal (Fig. 3D). Some of these cells were also tuned conjunctively to place (Fig. 3E and fig. S11); however, the path-distance tuning could not be explained by the place tuning (fig. S12).

Cells were more tuned to path distance than to time to landing (fig. S13), although both distance to goal and time to goal could be useful signals for navigation [with timing information possibly represented by time cells (*24*)]. The goal-distance cells were significantly more tuned to path distance than to Euclidean distance to the goal (fig. S14, A to D). During complex nonstraight flights, as in our experiment—or when flying in the wild through interconnected cave systems—the encoding of path distance may be particularly useful for guiding navigation. In contrast, during long-distance natural navigation, bats are known to fly in very straight lines (*25*), in which case the path distance would be similar to the Euclidean distance to the goal. Under the latter circumstances, neurons tuned to path distance and direction (Fig. 3D) might carry information about the length and angle of the vector to the goal. Further, we found that a subset of cells explicitly encoded the Euclidean distance to the goal (fig. S14E), often in conjunction with goal direction (Fig. 3F)—forming a full vectorial representation of the goal.

In summary, we report here on neurons that encode the egocentric direction (Fig. 1) and distance (Fig. 3) to navigational goals. We found these neurons in hippocampal area CA1, indicating

Downloaded from http://science.sciencemag.org/ on January 24, 2017

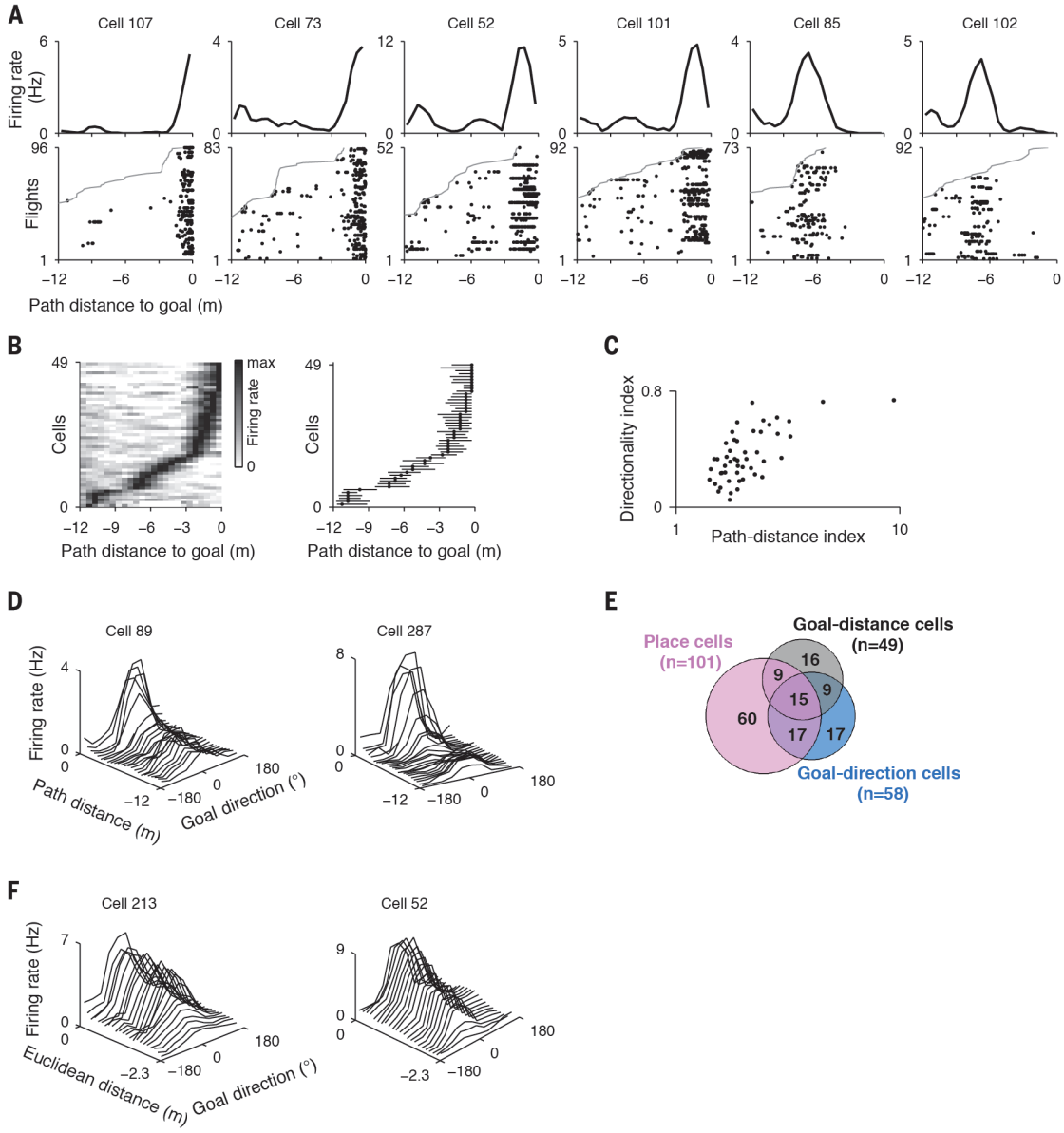

Fig. 3. Encoding of distance to the goal. (**A**) Six example neurons exhibiting tuning to path distance, sorted by preferred distance. Top, tuning curves (firing rate versus distance), computed from the rasters below (normalized by time spent at each distance). Bottom, raster plots of the last 12 m of path distance, aligned to landing (distance 0); black dots, spikes. Flights had different lengths and were sorted here by path distance; gray lines indicate flight start. (**B**) Tuning curves of all significant goal-distance cells ($n = 49$; sorted by preferred distance). Left, normalized distance-tuning curves for all cells (rows). Right, depiction of tuning widths (at half-height, lines) and preferred distances (dots). (**C**) Directionality index versus path-distance index for all goal-distance cells (Pearson correlation, $r = 0.65$, $P < 10^{-6}$; $n = 49$). (**D**) Tuning curves for two example cells conjunctively encoding goal direction and path distance to the goal. Plots depict firing rate as function of goal direction and path distance. (**E**) Total numbers of different functional cell types recorded in CA1. (**F**) Tuning curves for two example cells conjunctively encoding goal direction and Euclidean distance to the goal.

that the hippocampus contains a variety of navigation-related signals, including a place signal, a head-direction signal, and a vectorial representation of goals. The goal-direction and goal-distance tuning could not be explained by the classical CA1 place tuning (Fig. 1 and figs. S3, S4, and S12) or by the head-direction tuning (fig. S5). Notably, goal-direction neurons were able to represent occluded goals, suggesting that goal-direction tuning is memory-based rather than sensory-based (Fig. 2). Together, our data demonstrate genuine goal-direction and goal-distance signals in the hippocampus, constituting a vectorial representation of spatial goals.

The goal-direction cells are very different from hippocampal neurons reported previously in rats that fire on one side of a landmark but that are not affected by the animal's orientation relative to the landmark (*26*). In addition, the goal-direction signal was strongly affected when we moved the goal (Fig. 2); it is therefore goal-specific and conceptually different from spatial-view cells reported previously in monkeys, which are tuned to an abstract point on the wall (*27*). The goal-direction signal is memory-based (Fig. 2) and is thus different from cells found in the rat parietal cortex, which respond to the direction of visible cues (*28*).

We argue that the mammalian navigation system, which contains the major spatially tuned classes of cells in the brain (*1*, *4*, *6*), is incomplete without a representation of the goal location to which the animal is navigating. Our finding of a vectorial representation of goals in the hippocampus might fill this gap. The preferred goal directions spanned the entire range of 360° (Fig. 1, F and G), and therefore the goal-direction signal

Downloaded from http://science.sciencemag.org/ on January 24, 2017

can allow the bat to decode its deviation from the goal (e.g., during navigational detours) and thus to reach its goal; the additional presence of a distance signal may enable even more sophisticated computations. Our results are consistent with a recent functional magnetic resonance imaging study in humans, which reported hippocampal activation related to a combination of goal direction and path distance to the goal (*29*); importantly, here we demonstrate single neurons encoding goals in a vectorial manner in egocentric coordinates. We speculate that the hippocampal representation of hidden goals reported here might provide an unexpected explanation of why hippocampal lesions impair navigation to hidden goals (e.g., in a water maze) (*30*). Last, we propose that this neural representation could underlie the vector-based navigation strategies described for many species, from insects to humans (*14*–*19*)—suggesting a previously unrecognized mechanism for goal-directed navigation across species.

REFERENCES AND NOTES

1. J. O'Keefe, J. Dostrovsky, *Brain Res.* **34**, 171–175 (1971).
2. M. A. Wilson, B. L. McNaughton, *Science* **261**, 1055–1058 (1993).
3. N. Ulanovsky, C. F. Moss, *Nat. Neurosci.* **10**, 224–233 (2007).
4. T. Hafting, M. Fyhn, S. Molden, M.-B. Moser, E. I. Moser, *Nature* **436**, 801–806 (2005).
5. M. M. Yartsev, M. P. Witter, N. Ulanovsky, *Nature* **479**, 103–107 (2011).
6. J. S. Taube, R. U. Muller, J. B. Ranck Jr., *J. Neurosci.* **10**, 420–435 (1990).
7. A. Finkelstein *et al*., *Nature* **517**, 159–164 (2015).
8. B. E. Pfeiffer, D. J. Foster, *Nature* **497**, 74–79 (2013).
9. A. Johnson, A. D. Redish, *J. Neurosci.* **27**, 12176–12189 (2007).
10. B. L. McNaughton, J. J. Knierim, M. A. Wilson, in *The Cognitive Neurosciences*, M. Gazzaniga, Ed. (MIT Press, 1995), pp. 585–595.
11. N. Burgess, J. O'Keefe, *Hippocampus* **6**, 749–762 (1996).
12. D. Bush, C. Barry, D. Manson, N. Burgess, *Neuron* **87**, 507–520 (2015).
13. M. Stemmler, A. Mathis, A. V. Herz, *Sci. Adv.* **1**, e1500816 (2015).
14. M. Müller, R. Wehner, *Proc. Natl. Acad. Sci. U.S.A.* **85**, 5287–5290 (1988).
15. A. S. Etienne *et al*., *Nature* **396**, 161–164 (1998).
16. H. G. Wallraff, *Avian Navigation: Pigeon Homing as a Paradigm* (Springer, 2005).
17. C. R. Gallistel, *The Organization of Learning* (MIT Press, 1990).
18. R. F. Wang, E. S. Spelke, *Cognition* **77**, 215–250 (2000).
19. P. Foo, W. H. Warren, A. Duchon, M. J. Tarr, *J. Exp. Psychol. Learn. Mem. Cogn.* **31**, 195–215 (2005).
20. Materials and methods are available as supplementary materials.
21. A. Rubin, M. M. Yartsev, N. Ulanovsky, *J. Neurosci.* **34**, 1067–1080 (2014).
22. L. Acharya, Z. M. Aghajan, C. Vuong, J. J. Moore, M. R. Mehta, *Cell* **164**, 197–207 (2016).
23. H. Eichenbaum, N. J. Cohen, *Neuron* **83**, 764–770 (2014).
24. H. Eichenbaum, *Nat. Rev. Neurosci.* **15**, 732–744 (2014).
25. A. Tsoar *et al*., *Proc. Natl. Acad. Sci. U.S.A.* **108**, E718–E724 (2011).
26. S. S. Deshmukh, J. J. Knierim, *Hippocampus* **23**, 253–267 (2013).
27. P. Georges-François, E. T. Rolls, R. G. Robertson, *Cereb. Cortex* **9**, 197–212 (1999).
28. A. A. Wilber, B. J. Clark, T. C. Forster, M. Tatsuno, B. L. McNaughton, *J. Neurosci.* **34**, 5431–5446 (2014).
29. L. R. Howard *et al*., *Curr. Biol.* **24**, 1331–1340 (2014).
30. R. G. Morris, P. Garrud, J. N. Rawlins, J. O'Keefe, *Nature* **297**, 681–683 (1982).
31. A. Sarel, A. Finkelstein, L. Las, N. Ulanovsky, paper presented at the Annual Meeting of the Israel Society for Neuroscience, Eilat, Israel, 7 to 9 December 2014.

ACKNOWLEDGMENTS

We thank S. Romani, A. Treves, A. Rubin, T. Stolero, D. Omer, T. Eliav, G. Ginosar, D. Blum, and S. Maimon for comments on the manuscript; O. Gobi and S. Kaufman for bat training; A. Tuval for veterinary support; C. Ra'anan and R. Eilam for histology; B. Pasmantirer and G. Ankaoua for mechanical designs; and G. Brodsky and H. Avital for graphics. This study was supported by research grants to N.U. from the European Research Council (ERC-StG NEUROBAT and ERC-CoG NATURAL_BAT_NAV), the Israel Science Foundation (ISF 1319/13), and the Minerva Foundation. Equipment support was provided by the Krenter Institute at the Weizmann Institute of Science. The data are archived on the Weizmann Institute of Science servers and will be made available on request. The results reported in this study were presented earlier in abstract form (*31*).

SUPPLEMENTARY MATERIALS

www.sciencemag.org/content/355/6321/176/suppl/DC1
Materials and Methods
Figs. S1 to S14
References (*32*–*34*)

28 September 2016; accepted 14 December 2016
10.1126/science.aak9589

Downloaded from http://science.sciencemag.org/ on January 24, 2017

www.sciencemag.org/content/ 355/6321/176/suppl/DC1

Supplementary Materials for

Vectorial representation of spatial goals in the hippocampus of bats

Ayelet Sarel, Arseny Finkelstein, Liora Las, Nachum Ulanovsky*

*Corresponding author. Email: nachum.ulanovsky@weizmann.ac.il

Published 13 January 2017, *Science* **355**, 176 (2017)
DOI: 10.1126/science.aak9589

This PDF file includes:

Materials and Methods
Figs. S1 to S14
References

Materials and Methods

Subjects and behavioral setups

Three adult male Egyptian fruit bats (*Rousettus aegyptiacus*; weights 174–179 gr) were trained to fly in a large flight room (5.8×4.6×2.7 m) with a single goal positioned inside the room (see Figs 1A and 2A): The goal was either an elevated platform (size: 0.4×0.4-m, height above floor: 1.24 m) or an elevated sphere (0.15-m diameter, height above floor: 1.15 m). In the room we also positioned a curtain that was opaque to vision, echolocation and olfaction (size of curtain: 3.0-m length × 2.7-m height); the curtain was located in the same position across all behavioral sessions and across all experimental days (Fig. 2A; see below for session-descriptions). The bat flew freely in the room in complex and variable trajectories (fig. S1), and decided on its own volition when to land on the goal, where it found food-reward (small pieces of banana) and could rest until the next flight. We did not attempt to manipulate systematically the amount of reward in order to test its possible effects on neuronal responses – because for a flying bat it is quite rewarding to land on a goal to rest, and thus it is difficult to parameterize the "total reward size".

Bats' average speed in this task was 2.6 ± 1.3 m/s ; the average duration of individual flights was 7.7 ± 4.3 s ; and the average distance per flight was 16.4 ± 9.5 m (mean ± s.d.). These long flight-distances (which were confined within our 5.8 × 4.6-m flight-room) meant that the bat flew in complex curved trajectories inside the room, prior to landing (see example trajectories in Fig. 1A and fig. S1). The total duration of the behavioral experiment (all sessions) was typically 70–90 min, and it was flanked by two sleep sessions, before and after the behavior, lasting 5–10 min each (denoted as 'pre' and 'post' sleep sessions). Experiments were done under relatively dim light conditions (illuminance 2 lux).

The goal could be in one of two positions – either in a 'central' or in a 'hidden' position, in two different sessions (Fig. 2A):

"Central goal session": the goal was positioned in the center of the room (Fig. 2A-bottom, and Fig. 1A); experiments with central goal position were collected from all three bats. The location of the goal in the center of the room created a roughly omnidirectional behavior around the goal – which enabled dissociating the goal-direction representation from other neuronal representations, such as place-coding and head-direction coding (Fig. 1 and figs S3, S5).

"Hidden goal session": the goal was positioned behind the curtain (Fig. 2A-top). The first behavioral session, for two out of the three bats, was always a hidden-goal session, where the goal was occluded behind the curtain – while its exact location behind the curtain was randomly changed from day to day. The bat had to fly and reach the hidden-goal from the sides of the curtain, and thus quickly learned the daily location of the hidden goal. We note that the bat could *not* see the hidden-goal when it was flying in the central area of the room. In the second session we moved the goal to the center of the room, and conducted a central goal session (Fig. 2A, bottom; as described above). Note that both the bat's behavior and the neural recordings were continuous (i.e. we did not stop the recordings or interfere with the bat's behavior between sessions) – and the only change in the experimental setup was the change in the location of the goal.

The analyses for Figures 1 and 3 were done only based on the central-goal session. The analyses for Fig. 2 focused on comparing both kinds of behavioral sessions: i.e. the hidden-goal session versus the central-goal session. Experiments that included both a hidden-goal session and a central-goal session were conducted in two of the three bats (bats no. 2 and 3).

For one of the bats (bat no. 1) we conducted the experiment differently: in the first session we used the central goal, and in the second session we added another platform that was hidden behind the curtain. This experiment did not allow us to test the tuning to the hidden goal separately, because the two goals were present together in the second session; therefore, we did not use data from this bat for the hidden-goal analyses in Fig. 2 – but only for the central-goal analyses in Figs 1 and 3.

We also conducted an additional experiment in a fourth bat (adult male, weight 171 gr), in which there were two identical platforms simultaneously in the room throughout the recordings, and both platforms were always visible. We used the data from this animal (bat no. 4) only in fig. S12D-F, for dissociating distance-tuning from place-tuning (for more details, see the figure legend of fig. S12D-F).

Bats were maintained on a reversed light-dark cycle; all recordings were conducted during the dark phase. All experimental procedures were approved by the Institutional Animal Care and Use Committee of the Weizmann Institute of Science.

Surgery and recording techniques

After completion of training, bats were implanted with a four-tetrode microdrive (weight 2.1 gr), loaded with four tetrodes, each constructed from four strands of insulated wire (17.8 μm diameter platinum-iridium wire) – as described previously (*5, 7, 32*). Tetrodes were gold-plated to reduce wire impedance to 0.3–0.7 MΩ (at 1 kHz). The microdrive was implanted above the right dorsal hippocampus (3.6–3.75 mm lateral to the midline and 5.5–5.8 mm anterior to the transverse sinus that runs between the posterior part of the cortex and the cerebellum). The microdrive was attached to the skull using Superbond and dental acrylic, cemented to a set of

bone-screws; the craniotomy was sealed using Kwik-Sil. Surgical procedures were similar to those described previously (*5, 7, 32*), with the main difference being that we used here a new anesthesia protocol (*33*): we injected an anesthesia cocktail composed of Medetomidine 0.25 mg/kg, Midazolam 2.5 mg/kg and Fentanyl 0.025 mg/kg – and subsequently added-on additional injections as needed, based on monitoring the bat's breathing and heart-rate. At the end of the surgery bats were given the analgesic Metacam and the anti-inflammatory drug Dexamethasone. Following surgery, the tetrodes were slowly lowered toward the CA1 pyramidal layer; positioning of tetrodes in the layer was provisionally assessed by the presence of high-frequency field oscillations ("ripples") and associated neuronal firing, and was later verified histologically. For each bat, one tetrode was left in an electrically-quiet zone and served as a reference, and the remaining three tetrodes served as recording probes. During recordings, a wireless neural-recording device ('neural-logger') was attached to a connector on the microdrive. Signals from all 16 channels of the 4 tetrodes were amplified (×200) and bandpass filtered (300 – 7,000 Hz), and were then sampled continuously at 29.3 kHz per channel, and stored on-board the neural-logger. During subsequent processing, the neural recordings were further filtered between 600 – 6,000 Hz, and a voltage threshold was used for extracting 1-ms spike waveforms.

Spike sorting

All spike-sorting procedures were identical to those described previously (*3, 5, 32*). Briefly, spike waveforms were sorted on the basis of their relative energies and amplitudes on different channels of each tetrode. Data from all sessions – the behavioral sessions and the two sleep sessions – were spike-sorted together. Well-isolated clusters of spikes were manually selected, and a refractory period (<2 ms) in the interspike-interval histogram was verified. A total of 309 well-isolated cells were recorded from hippocampal area CA1 of three bats.

It is possible that some cells were recorded more than once across days. However, this possibility seems less likely in bats than in rodents because the CA1 pyramidal layer in bats is thicker than in rodents (thickness of CA1 in bats: ~200 μm, see Fig. 1D), and the tetrodes were moved daily. Nevertheless, we repeated the main analyses of the paper for a non-redundant subpopulations of cells (populations containing only one recording-day for each tetrode: fig. S11); these analyses yielded similar results to main Figures 1–3.

Video tracking and estimation of the position, head-direction and goal-direction of the bat

The bat's position was tracked using two cameras located at two of the upper corners of the room (Fig. 1A). The cameras were connected to a video-tracker system which tracked the position of bright light-emitting diodes (LED) connected to the neural-logger on the bat's head. The video data were sampled at a 25-Hz rate. The 3D position of the bat was reconstructed using the direct linear transform algorithm applied on data from both cameras (*32*). All analyses were done only on flight epochs that were defined by having linear speed greater than 25 cm/s. Analyses of all the behavioral and neural data were conducted using custom code written in Matlab.

We computed the azimuth heading-direction (φ) of freely flying bats, based on the position of the bat's head, using the following equation:

$$\varphi = angle(\Delta x + \Delta y * i)$$

where x, y are the position of the bat's head in space; Δx, Δy, are the changes in head-position between consecutive video frames (computed after mild smoothing); and i is $\sqrt{-1}$ (see full details in ref. (*7*)). The heading-direction is illustrated schematically in Fig. 1B; this variable was used for computing the goal-direction angle (see below) and for approximating the head-direction in fig. S5. We focused on heading-direction and not on head-direction, for two main

reasons: First, the heading-direction might be more relevant for guiding navigation. Second, it was not possible to track the head-direction because, in our large flight-room, the long distance between the bat and the cameras did not allow enough resolution to distinguish between multiple LED's on the bat's head, as needed for assessing head-direction.

Goal-direction (γ) was defined as the angle between the azimuth heading-direction of the bat (φ, described above) and the direction of the vector (α) connecting the position of the bat's head (x, y) with the position of the goal (x_G , y_G) in the azimuthal plane (Fig. 1B):

$$\alpha = angle((x_G - x) + (y_G - y) * i)$$

$$\gamma = \text{modulo}((\alpha - \varphi) + \pi, 2\pi) - \pi$$

Goal-direction tuning

Goal-direction tuning curves were computed for each neuron by counting the number of spikes in each azimuthal bin (18 bins, each with 20° width) and dividing it by the total time spent in that bin. The 1D tuning curves were smoothed using a rectangular window of size 3-bins, in a circular manner. Unvisited bins (where total time-spent, before smoothing, was < 1.5 s) were discarded from the analysis.

We defined a 'directionality index' as the Rayleigh vector (RV) length – also known as mean vector length – computed using the following equation:

$$RV = \frac{\pi}{n * \sin(\frac{\pi}{n})} \sum_{j=1}^{n} r_{\gamma_j} e^{-i\gamma_j} / \sum_{j=1}^{n} r_{\gamma_j}$$

Where n is the number of circular goal-direction bins; γ_j is the angle in radians of the j^{th} circular bin ($\frac{2\pi j}{n}$); and r_{γ_j} is the average firing-rate for each goal-direction angle (i.e., the n values of r_{γ_j} describe the full goal-direction tuning curve).

We fitted the 1D goal-direction tuning curves of the neurons with a 1D circular normal function, known also as von Mises function, which has the following form:

$$R_i(\gamma) = C_1 e^{\kappa \cos(\gamma - \gamma_i)} + C_2$$

Where γ is the preferred goal-direction of this neuron in radians, γ_i is the direction in radians of the i-th circular bin, and κ, C_1, and C_2 are constants. The preferred goal-direction angle of the neurons (e.g. Fig. 1G) was defined based on the peak firing-rate of the fitted von-Mises function.

The tuning modulation-depth was computed based on the von Mises fit, and was defined as the difference between the maximum firing-rate and the minimum firing-rate of the fit. The change in the tuning modulation-depth between the sessions (Fig. 2E) was defined as the contrast index (CI) of the tuning modulation-depth for the goal's spatial-position, with and without the goal present in this position:

$$CI = \frac{Tuning\ modulation\ depth_{with\ goal} - Tuning\ modulation\ depth_{without\ goal}}{Tuning\ modulation\ depth_{with\ goal} + Tuning\ modulation\ depth_{without\ goal}}$$

This contrast-index was computed separately for the central position (Fig. 2E, top) and for the hidden position (Fig. 2E, bottom). Note that for a cell tuned to the hidden goal, the tuning modulation depth 'with goal' was computed for session 1 (when the hidden goal was present); while for a cell tuned to the central goal, the tuning modulation depth 'with goal' was computed for session 2 (when the central goal was present). This index was computed only for cells with stable firing-rates between the pre and post sleep sessions (to rule out recording-instability).

Classification of goal-direction cells

To be classified as a 'goal-direction cell', a neuron had to meet all the following five criteria: (1) The directionality-index (Rayleigh vector length) of the goal-direction tuning curve was significant based on a shuffling procedure: For each neuron, we concatenated all the in-flight

spike sequences across all flight-epochs – and then rigidly time-shifted all the spikes by a random time-interval, in a circular manner (with the end of the session wrapped to the beginning). This preserved both the spike number and the temporal firing pattern, but dissociated the time of spiking from the animal's actual behavior. This procedure was repeated 1,000 times for each neuron. A neuron was defined as significantly tuned to goal-direction if its directionality index exceeded the 95^{th} percentile of the shuffled distribution for that session. (2) In addition, we required that the directionality-index of the goal-direction tuning curve must be higher than 0.25. (3) More than 50 spikes were emitted in-flight during the relevant behavioral session. (4) The neuron had to exhibit a stable goal-direction tuning curve during the recording, with Pearson correlation of $r > 0.5$ between the tuning curves computed separately for even-minutes and odd-minutes. (5) The neuron had a stronger goal-direction tuning than place tuning, based on a reconstruction analysis (goal/place index >1, see below). All these analyses were done for each behavioral session separately.

These criteria yielded $n = 58$ cells tuned significantly to the central goal, comprising 19% of our 309 recorded neurons (proportion of cells for each bat: 18%, 22% and 14%); and $n = 43$ cells tuned significantly to the hidden goal (proportion of cells for bats no. 2 and 3: 30% and 9%). For 53 cells (out of the 309 total neurons) we were able to record three sessions (of which 7 cells were tuned to the central goal and 8 cells were tuned to the hidden goal). Sessions 1 and 3 were hidden-goal sessions (e.g. Fig. 2D); all population analyses on curtain-experiments (e.g. Fig. 2E and figs S7, S8, S9, S11) included both of these sessions, and included only cells that were stable along the entire experiment (verified by stable spike-sorting and by comparing the firing-rates in the 'pre' and 'post' sleep sessions, namely the sleep sessions conducted before and after all the behavioral sessions).

Classification of place cells

The 2D spatial firing-rate map of each cell was computed by counting the number of spikes and the time spent in each spatial bin (bin size: 0.2×0.2 m; the 2D firing rate map was computed just for the *x* and *y* axes, disregarding the *z* axis; we focused on the horizontal *x*-*y* plane because the bats' behavior covered a rather narrow horizontal slab around the height of the goal: see fig. S2). We smoothed both maps with a Gaussian kernel window ($\sigma = 1.5$ bins) and divided bin-by-bin the smoothed 2D spike-count by the smoothed 2D time-spent. Bins with less than 0.5-s time spent (before smoothing) were discarded from the analysis, unless an adjacent bin was visited. Finally we computed the spatial information (SI, in units of bits/spike) of the firing-rate map, using the following (*34*):

$$SI = \sum p_i(\frac{r_i}{\bar{r}}) \log_2(\frac{r_i}{\bar{r}})$$

Where r_i is the firing rate of the cell in the i^{th} bin, p_i is the probability of the bat to be in this bin, and $\bar{r}$ is the mean firing-rate of the cell.

A cell was classified as a place-cell based on four criteria: (1) Significant spatial information based on a shuffling procedure (95$^{\text{th}}$ percentile significance threshold, as described above for the goal-direction tuning). (2) Spatial information >0.4. (3) More than 50 spikes in-flight during the relevant behavioral session. (4) Stability of the firing-rate map over even and odd minutes, with Pearson correlation of $r > 0.5$ between the maps. All these analyses were done for each behavioral session separately.

Reconstruction analysis

To examine the relation between the goal-direction signal and the place signal, we asked whether the goal-direction tuning can explain the neuron's place tuning, or vice versa. In particular,

inhomogeneous flight-behavior of the bat, whereby it flies in certain locations in the room at specific goal-direction angles, could potentially create sharp tuning curves for both signals (place and goal-direction) even if the neuron is truly tuned to only one of these signals. The following analysis was aimed to reveal the true underlying tuning of such cells (*21*). To this end, we first assumed that the cell is a pure place-cell, and based on this assumption and the animal's actual behavior we reconstructed what would be the expected goal-direction tuning; and conversely, we assumed that the cell is a pure goal-direction cell, and reconstructed the expected place-tuning. We then compared the quality of these two reconstructions. In order to do this comparison, we computed both the place-tuning and the goal-direction tuning using the same number of bins (20 bins).

The reconstructed (expected) place tuning $\hat{r}(x,y)$ was computed by assuming that the neuron is a pure goal-direction cell, using the following equation:

$$\hat{r}(x,y) = \frac{\sum_{\gamma}(p(x,y,\gamma) * r(\gamma))}{\sum_{\gamma}(p(x,y,\gamma))}$$

where $p(x,y,\gamma)$ is the fraction of time that the bat spent in each spatial bin at a specific goal-direction angle, γ, and $r(\gamma)$ is the firing-rate for this goal-direction γ. Then, the reconstructed place-tuning was compared to the observed place-tuning of the cell (fig. S3: top row in each example in panels B, D), using the normalized mean squared error (denoted below as 'error'). To this end, we first normalized both tunings to percentage from the peak; then we computed the error as follows:

$$Error = \frac{< (observed - expected\ )^2 >}{\max(observed) - \min(observed)}$$

where 'expected' is the reconstructed tuning.

For the converse reconstruction: The expected goal-direction tuning curve $\hat{r}(\gamma)$ was computed by assuming that the neuron is a pure place-cell, using the following equation:

$$\hat{r}(\gamma) = \frac{\sum_{x,y}(p(x,y,\gamma) * r(x,y))}{\sum_{x,y}(p(x,y,\gamma))}$$

where $p(x,y,\gamma)$ is the fraction of time that the bat spent in each spatial bin *x*,*y* at a specific goal-direction angle, γ, and $r(x,y)$ is the firing-rate for this spatial bin. Then the error between the reconstructed (expected) and the observed goal-direction tuning was computed as described above (fig. S3: bottom row in each example in panels B, D).

Next, in order to compare directly between the place signal and the goal-direction signal – i.e. to test if a neuron is more place-tuned or more goal-direction tuned – we compared between the errors of the two reconstruction procedures (see fig. S3E). Note that a lower error represents better reconstruction (smaller difference between observed and expected firing) – meaning that the signal that we used for the reconstruction explains better the firing of the cell. We defined a 'goal/place index' to quantify this comparison (Fig. 1I) – this index was defined as follows:

$$\frac{error\ assuming\ pure\ place\ tuning}{error\ assuming\ pure\ goal\ tuning}$$

To validate the performance of the analysis, we simulated pure place-cells: We generated spikes in a Poisson process based on a 2D Gaussian spatial tuning (centered for different simulations at every other spatial bin in the room), using the real flight behavior of the bat (taking the behavior from all days where goal-direction cells were recorded: n = 49 days; yielding a total of n = 5,625 simulated pure place-cells). The place-field size and peak firing-rate were based on the averages of the real place-cells in our data. This simulation showed that despite a possible behavioral inhomogeneity, the reconstruction analysis successfully reveals the

true underlying tuning of the cells – note that the simulated pure place-cells *all* had lower error for the reconstruction that assumed pure place-tuning (fig. S3E: all black dots are *below* the diagonal: n = 5,625 dots). Accordingly, all the simulated place cells had goal/place index < 1 in Fig. 1I (pink histogram).

The fifth criterion for the goal-direction cell classification (see above, section: "Classification of goal-direction cells") was to include only those cells that had lower error for the reconstruction which assumed pure goal-direction tuning, as compared with the error for the reconstruction which assumed pure place-tuning (i.e., cells that were above the diagonal in fig. S3E, that is: goal/place index >1). This very strict criterion verified that it is extremely unlikely that the goal-direction tuning of the goal-direction cells was a result of place-tuning ($P < 2\times10^{-4}$ for *all* the 58 goal-direction cells – see Fig. 1I).

Note that this reconstruction analysis has several advantages: First, it explicitly addresses the behavioral coupling between the position and the goal-direction. Second, it conserves the number of spikes. Third, the reconstruction analysis is model-free: the empirically-measured tuning curves serve as the model, and therefore do not require any model-fitting.

An analogous analysis was done also to dissociate the goal-direction tuning from the head-direction tuning (see fig. S5C).

In-field and out-of-field tuning of goal-direction cells

To determine whether the goal-direction signal is independent of the place signal, we computed the goal-direction tuning separately inside the place-field and outside the place-field (*21*). The in-field area was defined by computing the convex hull encompassing the set of spatial bins in which the firing-rate was greater than half of the peak firing-rate. Next, to make sure that we do

not include residual in-field spikes, we expanded the convex hull by two spatial bins in each direction (Fig. 1J-bottom, gray lines). The out-field area was defined as all the bins outside the in-field area (i.e. outside of the gray line, Fig. 1J-bottom). The goal-direction tuning was then computed separately for in-field spikes and behavioral data, and for out-field spikes and behavioral data (Fig. 1J – top plots, Fig. 1K and fig. S7D).

We conducted similar analysis to determine whether the goal-direction signal is independent of the head-direction signal. We computed the goal-direction tuning separately inside and outside the head-direction 'field'. The 'field' of the head-direction tuning was defined as ±60° from the angle with the maximal firing-rate in the head-direction tuning curve. We then computed the goal-direction tuning separately based on spikes and behavioral data that occurred in or out of the head-direction 'field' (fig. S5D).

These two analyses (Fig. 1J-K, fig. S5D and fig. S7D) were conducted for all the significant goal-direction cells.

Goal-direction tuning stability along the flight

To compute the stability of the goal-direction tuning along the flight (Fig. 1L and 1M- left), we first aligned all flights to the landing-time. Then we divided all flight trajectories to 26 time-bins of 0.3-s each – a total of 8 seconds (the last bin contained data also from longer flights; we used a rectangular sliding window of 2.5-s). Finally we measured the goal-direction tuning for each time-bin separately (using 10 bins of 36°), where bins with time-spent of less than 0.3-s were discarded from the analysis. To quantify the stability, the matrices of time by goal-direction (Fig. 1L) were divided into two (first half and second half of the flight); then we calculated the

Pearson correlation between the average goal-direction tuning that was computed for each half-matrix separately (see Fig. 1M, left).

Path-distance tuning

To compute the path-distance signal, all flights in which the bat landed on the central goal were aligned to the landing (distance 0). The total path-distance was defined as the total distance along the flight-trajectory – from takeoff to landing. The tuning curves were computed using a bin-size of 0.5 m: we divided the number of spikes in each bin by the total time spent in that bin, and smoothed with a window of length 3-bins (see e.g. Fig. 3A, top). Unvisited bins (where total time-spent, before smoothing, was < 1 s) were discarded from analysis. The average tuning and rasters are presented only for the last 12 meters of the flight (Fig. 3A and fig. S10).

To be classified as a 'goal-distance cell', a neuron had to meet all the following criteria: (1) The distance-tuning width (full width at half-maximum) was narrower than 3-m. (2) More than 50 spikes were emitted during the flights to the central goal. (3) More than 15 flight-passages with spikes occurred through the 'distance-field' of the distance-tuning curve (defined by the full width at half-maximum).

We defined a 'path-distance index' (PDI) as the ratio between the maximal firing-rate and the mean firing-rate of the path-distance tuning; this index was used as a measure of the sharpness of the distance-tuning (Fig. 3C and fig. S14B-D).

Goal-direction tuning along the distance to the goal

To depict the goal-direction tuning along the distance-to-goal (Fig. 3D,F), we first aligned all flight trajectories to the landing (distance 0). We then divided all flight trajectories into distance bins (23 bins; path-distance: 0.5-m bin size – a total distance of 12 meters; Euclidean-distance:

0.1-m bin size – a total distance of 2.3 meters; the last bin contained data also from longer trajectories; we used a rectangular sliding window of 3.5-m for the path-distance and 0.6-m for the Euclidean-distance). Finally, we measured the goal-direction tuning for each distance-bin separately (using 10 bins of 36°). Direction × distance bins with time-spent of less than 0.3-s were discarded from the analysis.

Distance tuning inside the place-field and outside of the place-field

To determine whether the path-distance tuning is independent of the place signal, we computed the path-distance tuning separately inside the place-field and outside the place-field. The in-field and the out-of field areas were defined in the same way as described above for the goal-direction tuning in/out of the place field (described in the section: "In-field and out-of-field tuning of goal-direction cells"). Then, the path-distance tuning was computed separately using the in-field spikes and behavioral data and the out-field spikes and behavioral data (fig. S12A: gray and green tuning curves).

This analysis was conducted for all the goal-distance cells (n = 49).

Place tuning in- versus out- of the 'path-distance field'

To further dissociate between the distance tuning and the place tuning, we did also the converse analysis: We computed the place tuning separately for spikes that occurred inside the path-distance field and outside of the path-distance filed. The path-distance 'field' was defined by the width at half of the maximum firing-rate, and adding margins of 0.25-m (half-bin) in each direction (fig. S12C, top – gray vertical lines denote the path-distance fields). Then we computed

the spatial firing-rate maps separately for the spikes and behavioral data that occurred in- versus out- of the path-distance field (fig. S12C).

Time-to-landing tuning

To compare between the tuning to path-distance and the tuning to time-to-landing (fig. S13), we computed the time-to-landing tuning with the same number of bins as for the path-distance tuning (24 bins); the range of time was defined as the range of the path-distance (12 m) divided by the average speed of the bats (2.6 m/s). Tuning curves were computed similarly to path-distance tuning, by aligning all flights to landing (time 0).

To be classified as a 'time-to-landing cell', a neuron had to meet all the following criteria: (1) The time-to-landing tuning width (full width at half-maximum) was narrower than 1.15-s (defined by taking the threshold for path-distance cells, 3-m, and dividing it by the average speed, 2.6m/s). (2) More than 50 spikes were emitted during the flights to the central goal. (3) More than 15 flight-passages with spikes occurred through the 'time-field' (defined by the width at half of the maximum firing-rate).

Euclidean-distance tuning

To compare between the tuning to path-distance and the tuning to the Euclidean-distance to the goal (fig. S14), we computed both tuning-curves using the same number of bins (16 bins). Because each signal has a different distance-range, it created different bin sizes (path-distance bin size: 0.5-m; we used 8-m range in this analysis; Euclidean-distance bin size: 0.2-m, this number was obtained by taking the median of the experimentally-measured Euclidean distances in our flight room, 3.2-m, and dividing it into 16 bins). We computed the tuning by counting the

number of spikes in each bin and dividing it by the total time spent in that bin. Unvisited bins (where total time-spent, before smoothing, was < 1 s) were discarded from analysis. The 1D tuning curves were smoothed using a rectangular window of size 3-bins.

We defined a 'Euclidean-distance index' (EDI) as the ratio between the maximal firing-rate and the mean firing-rate of the Euclidean-distance tuning (fig. S14B-D); this index was used as a measure of the sharpness of the tuning.

Histology

Histology was done as described previously (*5*, *32*). Briefly, at the end of recordings, we did electrolytic lesions to mark the tetrode tips (DC positive current of 30 μA, 15-s duration), while the bat was anesthetized. Then, bats were given an overdose of sodium pentobarbital and were perfused transcardially using 4% paraformaldehyde or 4.5% histofix. Brains were removed and sectioned coronally (with 30-μm intervals). The sections were Nissl-stained with cresyl violet and were photographed. Using the lesion-marks we reconstructed the tetrode tracks and verified their locations in dorsal CA1.

Supplementary figure 1

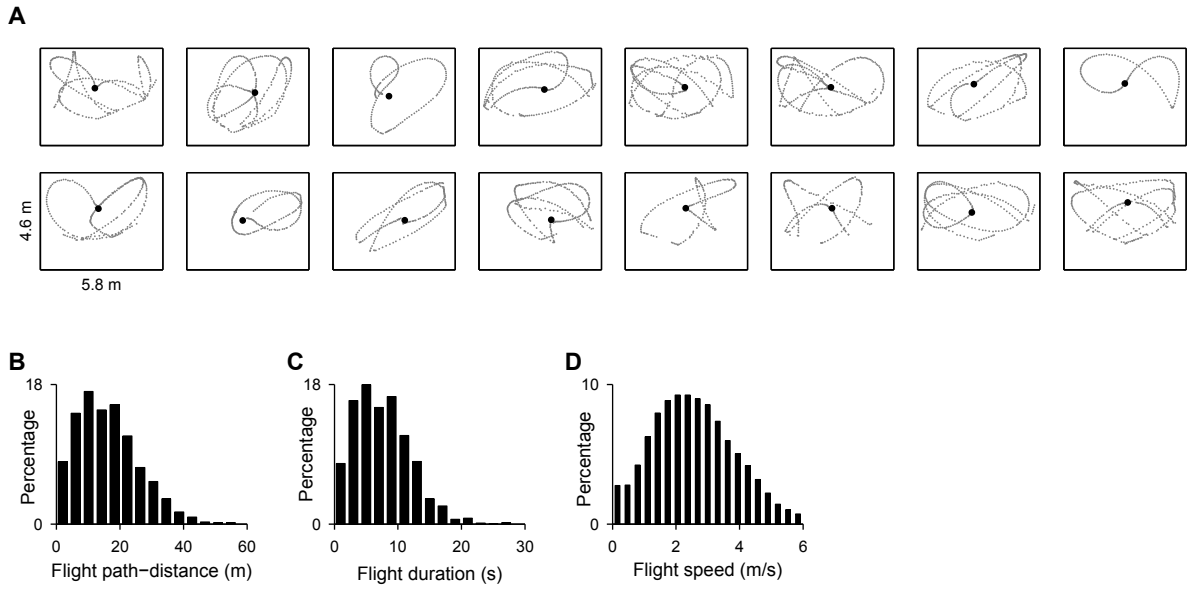

fig. S1. Bats exhibited highly-complex and long flights. (**A**) Examples of typical individual flight trajectories in this task (examples taken from all three bats). (**B-D**) distributions of different flight parameters, pooled over all bats and all days in which we recorded significant goal-direction cells (total *n* = 49 days). (**B**) Distribution of flight path-distance (i.e. total length of individual flights; mean ± s.d.: 16.4 ± 9.5 m). (**C**) Distribution of individual flight durations (mean ± s.d.: 7.7 ± 4.3 s). (**D**) Distribution of flight speed (mean ± s.d.: 2.6 ± 1.3 m/s).

Supplementary figure 2

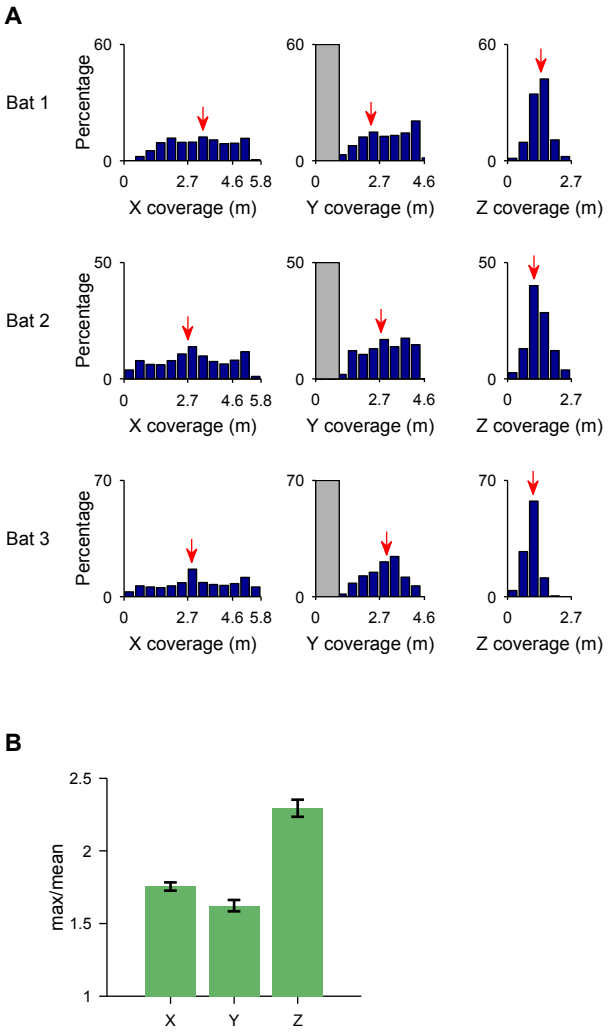

fig. S2. Behavioral coverage is not uniform in 3D: bats covered a rather narrow horizontal slab around the height of the goal. (**A**) Distribution of behavioral coverage during flight – the percentage of time spent by the bat at each location along the three dimensions of the room, shown for several example days. Each row shows data from a different bat. Left column, behavioral coverage in the X dimension of the room (size: 5.8 m); middle column, for the Y dimension (4.6 m); right column, for the Z dimension (2.7 m). The location of the goal in each dimension is marked by the red arrow. The left-gray rectangle in the Y histogram marks the area outside the view of the cameras (see main Fig. 1A). Note that in all three bats, in this behavioral setup the distribution in X and Y was relatively uniform – signifying a uniform behavioral coverage in the horizontal X-Y plane; while in the Z dimension the distribution was less uniform, and was concentrated around the goal height (red arrow in Z) – signifying that the bat flew in a rather narrow horizontal slab around the Z-height of the goal. (**B**) Population quantification of the uniformity of coverage in X and Y, and the 'peakiness' of coverage in Z: Plotted is the ratio between the maximum of the histogram divided by the mean of the histogram (not including the region of the gray rectangle in Y). Error-bar, population average ± s.e.m., pooling over all bats and all days in which we recorded goal-direction cells (total n = 49 days). The ratio in the Z dimension was significantly higher than in the other two dimensions (t-test comparing Z and X: $P < 10^{-12}$; t-test comparing Z and Y: $P < 10^{-13}$) – indicating that the Z-dimension in this behavioral setup was significantly less uniformly covered as compared to the X and Y dimensions.

Supplementary figure 3 - page 1

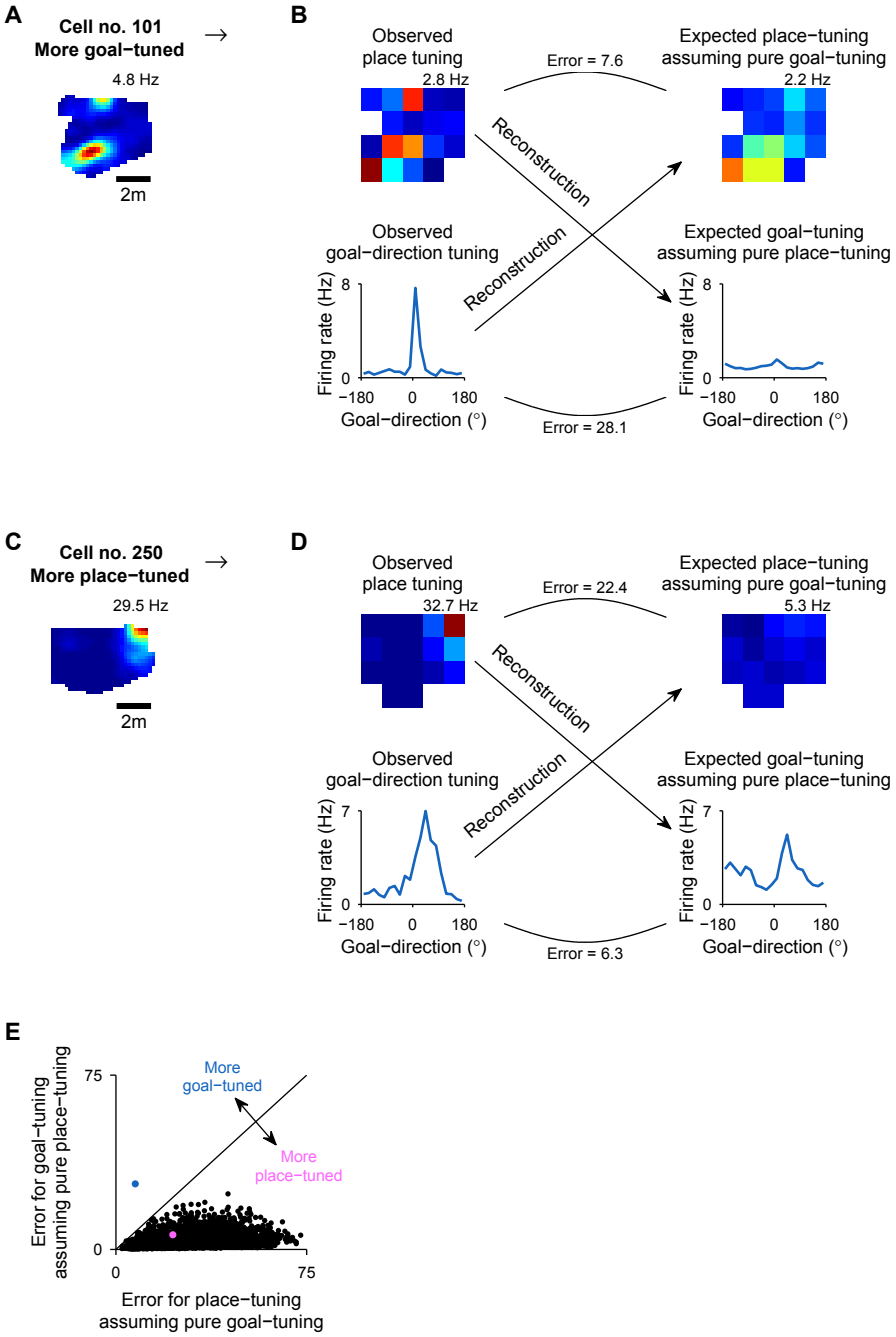

fig. S3. Reconstruction analysis shows that goal-direction tuning could not be explained by pure place-tuning. (**A**,**C**) Firing-rate maps plotted with regular bin size (0.2×0.2 m) for two example cells, which are further analyzed in B and D. (**B**, **D**) Examples of reconstruction analysis for a goal-direction cell (B) and a place cell (D). Top row: firing-rate maps, plotted with large spatial bins: Left – observed place tuning (a coarse binning of 1.15×1.15 m was used in order to yield 20 bins, which is the same number of bins as for the goal-direction tuning, which allows direct comparisons); Right – expected place tuning, based on the assumption that the cell is a pure goal-direction cell (using the observed goal-direction tuning – bottom left panel). To evaluate the performance of the reconstruction procedure, the normalized mean squared error (denoted as 'Error': see Methods) was computed between the observed and expected firing-rate maps. Bottom row: goal-direction tuning: Left – observed goal-direction tuning (18° bin size; 20 bins, allowing comparison with the place-tuning); Right – expected goal-direction tuning based on the assumption that the cell is a pure place-cell (using the observed place tuning – top left panel). The error was then computed between these two goal-direction tuning curves. Both cells (in B and D) appear

Supplementary figure 3 - page 2

Continued from the previous page

to be conjunctive for place × goal-direction; however, comparing the errors of the two reconstruction procedures (assuming pure goal-tuning versus assuming pure place-tuning) reveals that cell no. 101 (B) had a much lower error under the assumption that the cell is a pure goal-direction cell – signifying that the firing of this neuron is better explained by the goal-direction tuning. By contrast, cell no. 250 (D) had lower error under the assumption that the cell is a pure place-cell – signifying that the firing of this neuron is better explained by the place tuning. (**E**) Distribution of errors for all the simulated pure place-cells (black dots; simulated using the real behavior of the bat for all days and all possible locations in the room, *n* = 5,625 simulated cells). Shown are also the example cells from B (blue) and D (pink).

Note that all the simulated place-cells fall below the identity-line ('goal/place index' < 1; see Methods), meaning that for all the simulated pure place-cells the reconstruction yielded a lower error when assuming pure place-tuning – confirming that the underlying tuning of these neurons was the place-tuning: as indeed we created them. We note that the fifth criterion we used for the classification of goal-direction cells was to have lower error in the reconstruction when assuming pure goal-direction tuning ('goal/place index' > 1 ; e.g. the blue dot in panel E). This very strict criterion verified that the goal-direction signal underlies the tuning of all the goal-direction cells reported in this study – and that the tuning of all the goal-direction cells could not be explained by pure place-tuning (see clear separation of histograms in Fig. 1I).

Supplementary figure 4

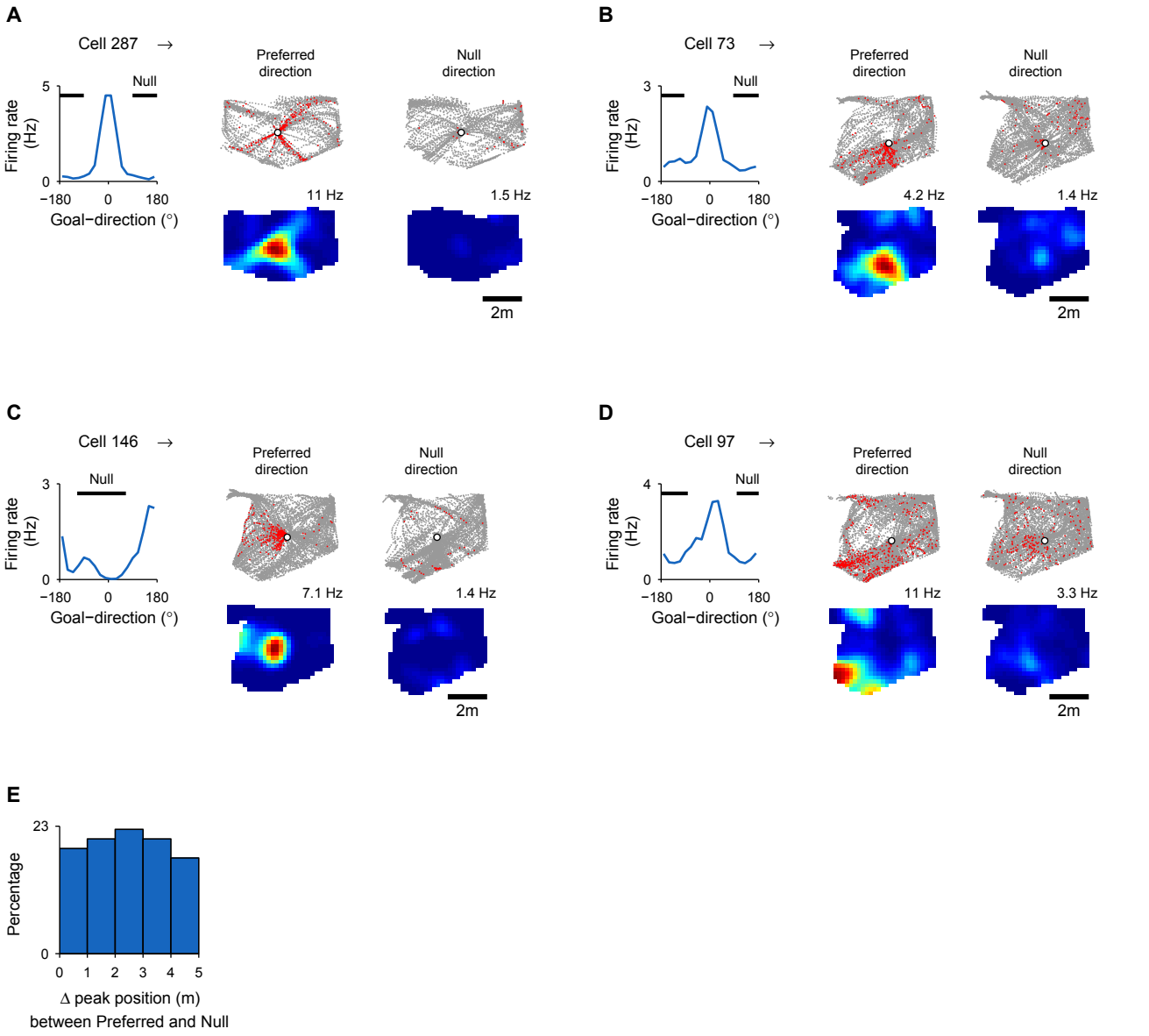

fig. S4. Place tuning almost vanishes in the null direction of goal-direction cells – i.e. at 180º from the preferred goal-direction. (**A**-**D**) Examples of place-tuning in the preferred versus null goal-directions for 4 cells which were carrying both goal-direction and place signals. For each neuron: Left – goal-direction tuning curve (black horizontal line indicates the region of the null direction [180º from the preferred-direction, and spanning ± 90º]). On the right shown are four spatial plots: Top two plots – positional coverage (gray) with spikes overlaid (red), plotted separately when the bat was in the preferred goal-direction (middle) or the null direction (right). Bottom two plots: corresponding firing-rate maps. Note the prominent reduction in firing-rate within the neurons' place-field when the bat was flying in the Null direction – i.e., these neurons are not classical place cells. Scale bar, 2-m (same scale-bar in panels A-D). (**E**) Distribution of distances between the peak-firing locations in the spatial firing-rate maps computed for the preferred goal direction versus the null direction (n=58 goal-direction cells). For each neuron, we compared the locations of peak-firing when the bat was in the preferred goal-direction (e.g. bottom rows in panels A-D: left) versus when it was in the null goal-direction (e.g. bottom rows in A-D: right). Note that the distances in this population histogram are rather uniformly distributed, and that the spatial shifts in some cells could be very large, oftentimes several meters in size. These large spatial shifts as function of goal-direction suggest that these neurons are not classical place cells.

Supplementary figure 5

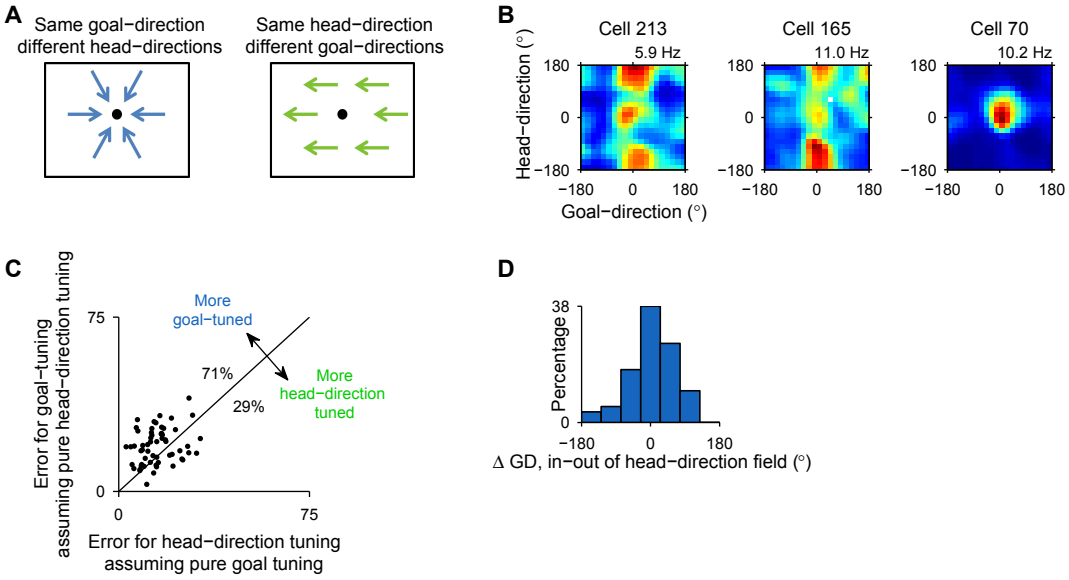

fig. S5. Goal-direction tuning is not explained by head-direction tuning. (**A**) Schematic drawing of the flight-room, showing that the egocentric goal-direction and the allocentric head-direction are different variables: The goal was positioned in the center of the room to enable dissociation between the head-direction and the goal-direction. Note that the two variables could be very different from each other: e.g., the bat could be in the same goal-direction angle but in different head-direction angles (in the left example: goal-direction 0°); and conversely, it could be in the same head-direction but in different goal-direction angles (in the right example: head-direction 180°). (**B**) Firing-rate maps for head-direction and goal-direction angles (bin size: 18°×18°), for 3 example neurons. Bins with time-spent less than 0.5-s were discarded from the analysis, unless the adjacent bin was visited. We smoothed the map with a Gaussian kernel window (σ=1.5 bins). The two left examples are for goal-direction cells without clear head-direction tuning (note vertical elongation); the right-most example is for a cell carrying both goal-direction and head-direction signals. Color scale goes from zero (blue) to maximal firing-rate (red; value indicated). (**C**) Population scatter for all the goal-direction cells (n = 58 neurons), showing the error values in the reconstruction analysis – comparing between the goal-direction signal and the head-direction signal for each neuron (dots). Note that 71% of the cells (41 of 58) were above the identity line, indicating that the cells' firing was explained better by the goal-direction tuning than by the head-direction tuning. (**D**) Distribution of the differences in preferred goal-direction (GD) angle between the in-'field' and out-of-'field' of head-direction tuning, for all goal-direction cells (n = 58). The narrow distribution, with a peak around 0°, suggests that for most of the goal-direction cells, the goal-direction tuning was similar between in-'field' and out-of-'field' of the head-direction tuning.

Supplementary figure 6

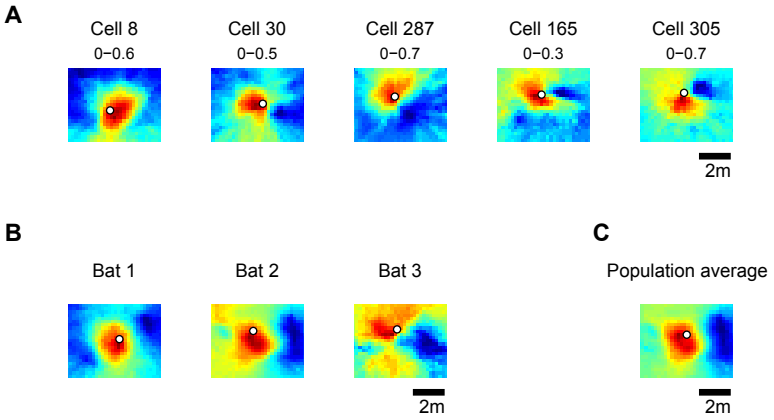

fig. S6. Goal-direction cells are specifically tuned to the goal and not to other locations in the environment. (**A**) Example goal-direction cells: Each spatial bin in the room (0.2 × 0.2-m bin size) was regarded here as a 'potential goal', and a goal-direction tuning curve was computed for each bin and quantified by the directionality index (Rayleigh vector length). The heat-map shows the directionality index for each spatial bin (the numbers above each plot indicate the range [minimum to maximum] of directionality-index values in each heat-map). Note the highest values of directionality index (red spot) are in the vicinity of the true goal (white circle; note the goal location was slightly moved between days) – indicating that the tuning is specific to the goal that was placed in the room by the experimenter, and not to other locations in the room. (**B-C**) Population average for goal-direction cells, computed by weighting each neuron's heat-map (as in A) by the spatial information of that map. White circles denote the average goal location across days for each bat (B) and pooled for all bats (C); note the goal location was slightly different between bats. The population average was most sharply tuned to the true goal location (white circle), as compared to other locations in the room. (**B**) Population average for all goal-direction cells, for each bat separately. (**C**) Population average over all the goal-direction cells pooled together. Scale bar, 2-m (same scale-bar in panels A-C).

Supplementary figure 7

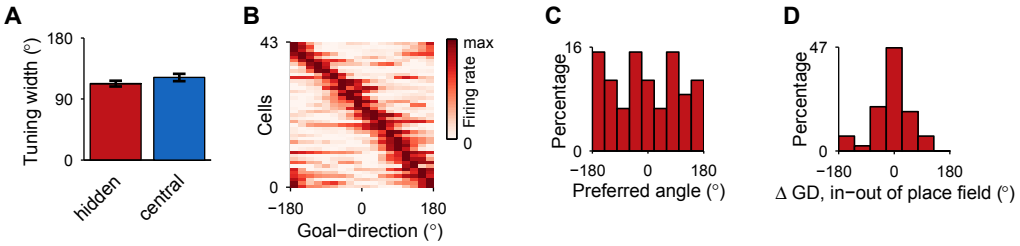

fig. S7. Properties of goal-direction cells that were tuned to the hidden goal.
(**A**) Average tuning width (mean ± s.e.m.) for all the goal-direction cells significantly tuned to the hidden goal (43 cells, for 3 of which we had two significantly-tuned sessions, yielding n = 46 tuning-curves), versus all the goal-direction cells significantly tuned to the central goal (n=31; here we took only cells from the 2 bats that performed the curtain experiment). Tuning width was computed based on the von-Mises fit (Methods) and was defined as the width of the tuning curve at half of the maximum height, where the height was measured from the peak firing-rate to the minimal firing-rate. There was no significant difference in tuning-width between the two goals (t-test: P = 0.18). (**B**) Normalized goal-direction tuning for all the goal-direction cells that were tuned to the hidden goal (n = 43); each row represents one cell (for those cells that had two hidden sessions with significant goal-tuning, we plotted here only the first hidden session). (**C**) Distribution of preferred goal-direction angles for all the goal-direction cells tuned to the hidden goal. During flights to the hidden goal, in this setup, the bat had to make detours to reach the goal (it could *not* fly straight to the goal through the curtain) – which may explain why it is useful to represent all possible angles, i.e. have a uniform distribution for the hidden goal (as compared to the central goal distribution in Fig. 1G). (**D**) Distribution of the difference in preferred goal-directions (GD) between in- and out- of the place field, for all goal-direction cells tuned to the hidden goal (similar analysis to main Fig. 1K). The narrow distribution with a peak around 0° suggests that for most of the goal-direction cells, the goal-direction tuning was similar in and out of the place-field.

Supplementary figure 8

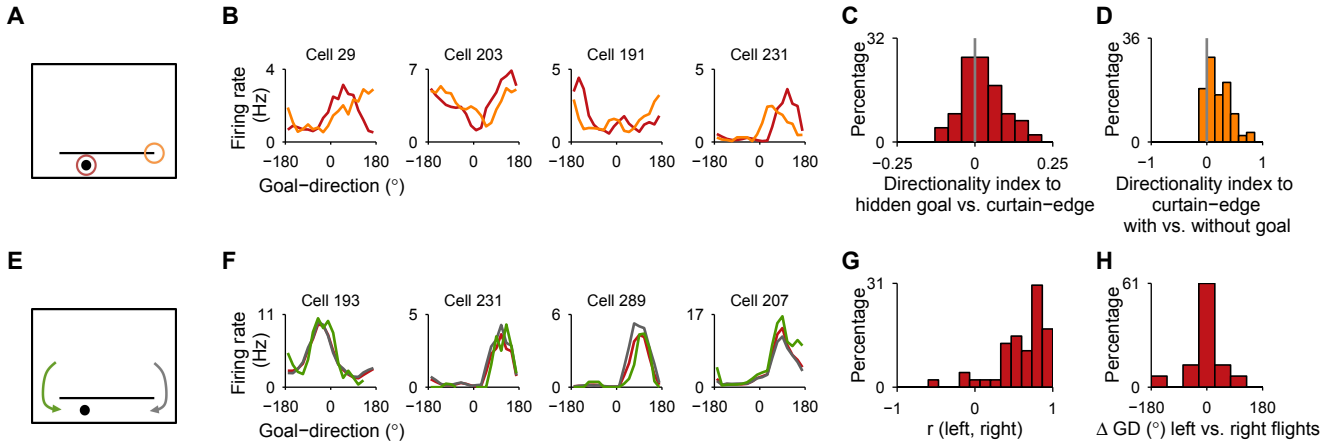

fig. S8. The tuning to the hidden goal is "through the wall". (**A**) Behavioral setup, showing top-view of the flight-room, with one goal (black filled circle) and an opaque curtain (black horizontal line). Red and orange circles represent, respectively, the goal and the curtain-edge position for which we computed the tuning curves in panel B. (**B**) Examples of goal-direction cells tuned to the hidden goal (red); these cells showed broader tuning-curves when the tuning was computed to the faraway curtain edge (orange; in this analysis we treated the curtain-edge as if it was a 'goal'). This broadening was quantified in panel C. Note that although we used the faraway curtain edge in this analysis, the hidden goal and the curtain-edge were still relatively close to each other (in the same overall part of the room), and therefore the observed tuning to the curtain-edge was likely a result of its relative proximity to the goal-location (see also control analysis in D). (**C**) Distribution of contrast indices between the directionality-indices, D, computed to the hidden goal versus the curtain-edge: $(D_{\text{hidden goal}} - D_{\text{curtain edge}}) / (D_{\text{hidden goal}} + D_{\text{curtain edge}})$. Cells were significantly more tuned to the hidden goal than to the curtain edge – as indicated by the rightward shift of the contrast-index distribution, compared to zero (indicated by the gray line; t-test: $P < 0.03$). (**D**) To test if the observed tuning to the curtain-edge was indeed a result of proximity to the hidden-goal location, we compared the tuning to the curtain-edge between the behavioral sessions (i.e. with versus without the goal being behind the curtain). Plotted is the distribution of contrast indices between the directionality-indices, D, that were computed to the same curtain-edge with versus without the goal in the hidden position: $(D_{\text{with goal}} - D_{\text{without goal}}) / (D_{\text{with goal}} + D_{\text{without goal}})$. Cells were significantly more tuned to the curtain edge when the goal was in the hidden position (t-test: $P < 10^{-12}$). Note that the curtain was always in the same position, and the bat flew behind the curtain many times in both sessions. This suggests that the changes in tuning to the curtain-edge resulted from the removal of the hidden-goal – and that the observed tuning to the curtain edge in the hidden-goal session (panel B, orange tuning curves) was likely caused by the relative proximity to the hidden-goal. (**E**) To further verify that the tuning was indeed for the hidden goal and not for the curtain-edges, we tested if there is a dependency of the goal-direction tuning on the direction from which the bat entered behind the curtain. Therefore, for the analyses in F-H, we divided the data to flights when the bat was eventually flying to the hidden-goal from the left entrance (green) or from the right entrance (gray) – see schematic trajectories. (**F**) Examples of goal-direction cells tuned to the hidden goal (red), showing similar tuning when flying to the goal from the left entrance behind the curtain (green) or the right entrance behind the curtain (gray). Note that the tuning-curves did *not* change depending on the trajectory of the bat to the hidden goal, i.e. whether the bat was flying to the goal from the left or the right side of the curtain – suggesting that the tuning is to the goal-position and not to the curtain edges. (**G**) Distribution of Pearson correlation coefficients between the tuning curves when the bat was flying to the hidden-goal from the left versus the right side of the curtain (i.e. correlations of green versus gray curves in panel F). Note the high correlation values. (**H**) Distribution of the differences in preferred goal-directions (GD) between the tuning-curves computed for flights from the left versus right sides of the curtain (green versus gray in E,F). Note the small values of the differences in preferred directions.

Overall these results suggest that the tuning to the hidden goal is "through the curtain" – not to curtain edges, nor to any odors that may come around the curtain edges.

Supplementary figure 9 - page 1

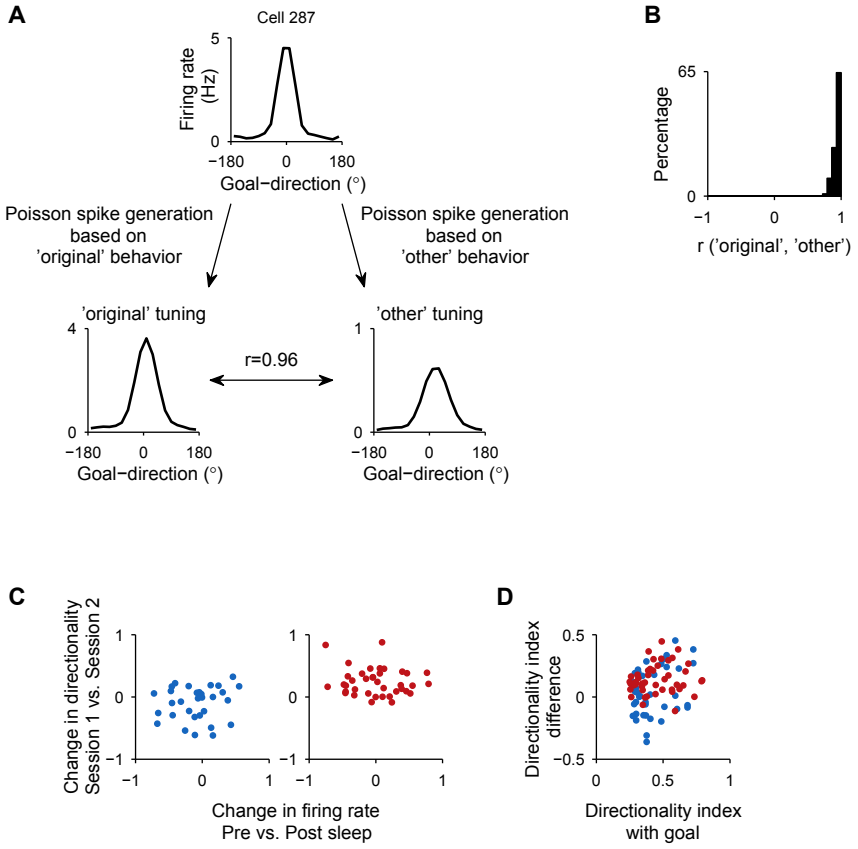

fig. S9. Changes in goal-direction tuning after the goal was moved did not result from changes in the behavior, nor from recording-stability, nor selection-bias. (**A**) Here we examined whether behavioral changes between sessions might underlie the dramatic changes in tuning that we observed between the sessions (Fig. 2). To this end, we tested whether it would be possible to obtain the goal-direction tuning of one of the sessions, called 'original' session, using the bat-behavior and mean-firing-rate taken from the 'other' session. In panel A, we show an example of this analysis for a goal-direction cell. Top: goal-direction tuning curve of cell no. 287 in one of the sessions. Based on this tuning curve, we generated the lower two goal-direction tuning curves based on a Poisson process, using: (1) the behavior and firing-rate of the original session (left tuning curve), or (2) using the behavior and firing-rate of the same cell in the 'other' session (right tuning curve). Both tuning curves were computed based on the average of 100 repeats of the Poisson spike-generation process. (**B**) Distribution of Pearson correlation coefficients between the 'original' and the 'other' goal-direction tuning curves (for the analysis described in A). Note the high correlations, indicating that it is possible to obtain the tuning curve of the original session based on the behavior of the animal and the mean firing-rate taken from the *other* session – signifying that the large changes in tuning-curve that we empirically observed when the goal was moved (Fig. 2) were *not* caused by changes in behavior, nor from chance differences in the firing-rate between the two sessions. (**C**) To verify that the observed changes in goal-direction tuning when the goal was moved (Fig. 2) were not a result of recording instability (slow drift in firing-rate along the recording), we did the following. We tested whether there is a correlation between the change in directionality and the change in recording stability – as quantified by the overall change in firing-rate between the two sleep sessions ('pre' and 'post') that were conducted before and after the behavioral experiment. The firing-rate (*FR*) change between the 'pre' sleep and 'post' sleep was defined using the following contrast index: $(FR_{\text{pre sleep}} - FR_{\text{post sleep}}) / (FR_{\text{pre sleep}} + FR_{\text{post sleep}})$. The directionality change was defined through the following contrast-index: $(D_{\text{session 1}} - D_{\text{session 2}}) / (D_{\text{session 1}} + D_{\text{session 2}})$, where *D* denotes the directionality (i.e. the Rayleigh vector length). Note that both of these contrast-indices are computed in chronological order, to test if a higher directionality could result from a higher firing-rate in the adjacent sleep session (signifying recording instability). Because the directionality change was

Supplementary figure 9 - page 2

Continued from the previous page

computed between session 1 and session 2, neurons tuned to the central goal (left – blue scatter) had on average a lower contrast index, because they have higher directionality in session 2 when the central goal was present; and conversely, neurons tuned to the hidden goal (right – red scatter) had a higher contrast index, due to higher directionality in session 1 when the hidden goal was present. This analysis shows that there was no significant correlation between the firing-rate changes and the directionality changes (Pearson correlation coefficients for these two scatter-plots: blue scatter [cells tuned to the central-goal]: $r = 0.12$, $P = 0.52$; red scatter [cells tuned to the hidden-goal]: $r = –0.13$, $P = 0.43$). This lack of correlations suggests that the tuning-changes that we observed when the goal was moved did *not* result from an overall slow change in firing-rate during the recordings (i.e., recording-instability). (**D**) Testing for a possible selection-bias in Fig. 2E. In Figure 2E (as in all other goal-direction analyses), we used our standard selection criteria for goal-direction cells (Methods) – meaning that we selected cells with relatively high directionality index in the relevant session (high $D_{\text{with goal}}$). Therefore, a possible concern is that the observed change in tuning modulation-depth (Fig. 2E) could be a "regression-to-the-mean effect" – i.e. cells with high $D_{\text{with goal}}$ would tend to have $D_{\text{without goal}}$ that is closer to the population mean. This, in turn, would imply that cells with high $D_{\text{with goal}}$ will have higher difference between the directionality indices with and without the goal. Here we directly tested this concern, by plotting a scatter of the differences in directionality index ($D_{\text{with goal}} – D_{\text{without goal}}$) versus the directionality index with the goal ($D_{\text{with goal}}$). Contrary to what would be expected from selection-bias, there were no significant correlations between the difference in directionality-index and the directionality-index with the goal (Pearson correlation coefficients for these two scatter-plots: red scatter [cells tuned to the hidden-goal]: $r = 0.16$, $P = 0.29$; blue scatter [cells tuned to the central-goal]: $r = 0.31$, $P = 0.0503$). This lack of correlations suggests that the tuning-changes that we observed when the goal was moved (Fig. 2E) did *not* result from a selection bias (i.e. from "regression-to-the-mean").

Supplementary figure 10

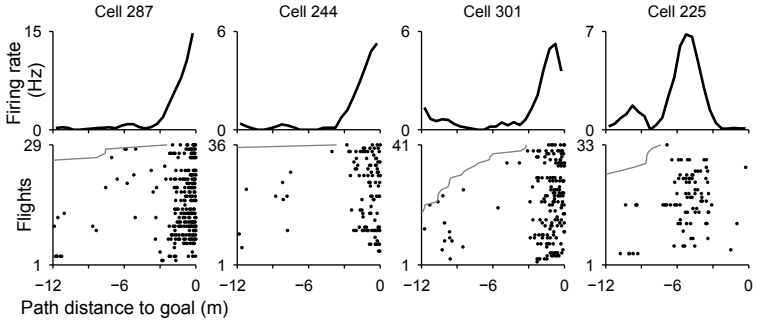

fig. S10. Examples of cells tuned to path-distance. Four example cells encoding the path-distance to the goal. Bottom, raster plot throughout the last 12 meters of path-distance, i.e. from –12 m until 0 m (aligned to landing: distance 0). Black dots, spikes; gray line, flight-start; flights were sorted by their total path-distance. Top, tuning curves: firing-rate versus distance, computed from the rasters below (normalized by time-spent in each distance). Note that cells 287, 244 and 301 (as well as the leftmost 4 examples in Fig. 3A) fired maximally when the bat approached the goal; while cell 225 (and the rightmost 2 examples in Fig. 3A) fired maximally at around –5 to –8 meters before landing.

Supplementary figure 11

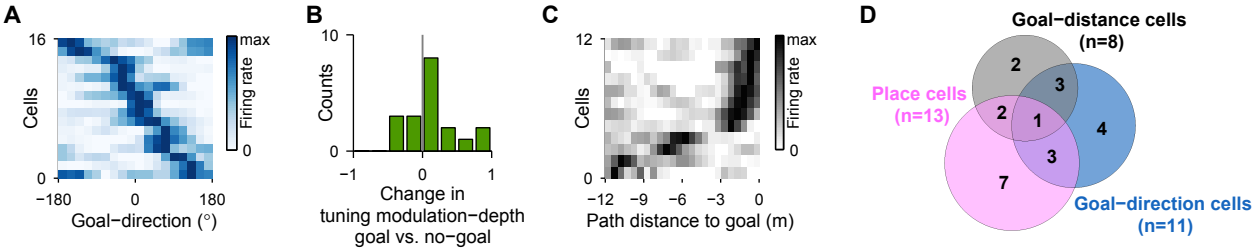

fig. S11. Main results hold for non-redundant subpopulations of recorded cells. (**A**) Normalized goal-direction tuning for a population of goal-direction cells recorded on one day from each tetrode (*n* = 16 cells; rows – sorted by preferred direction; similar to Fig. 1F). One recording-day for each tetrode was chosen based on maximal number of cells tuned to the central goal. (**B**) Distributions of changes in tuning modulation-depth – comparing the tuning to the same location with versus without a goal for all cells tuned to the central goal (*n* = 8 cells, 4 of them recorded for 3 sessions) or the hidden goal (*n* = 5 cells, 2 recorded for 3 sessions; similar to Fig. 2E). One recording-day per tetrode was chosen based on maximal number of cells tuned to the central or the hidden goal. (**C**) Normalized distance-tuning curves for a population of goal-distance cells (rows) recorded on one day from each tetrode (similar to Fig. 3B). One recording-day per tetrode was chosen based on maximal number of cells tuned to path-distance. (**D**) Total numbers of different functional cell types recorded on one day for each tetrode in CA1 (similar to Fig. 3E). One recording-day per tetrode was chosen based on maximal total number of cells recorded on each tetrode.

Supplementary figure 12 - page 1

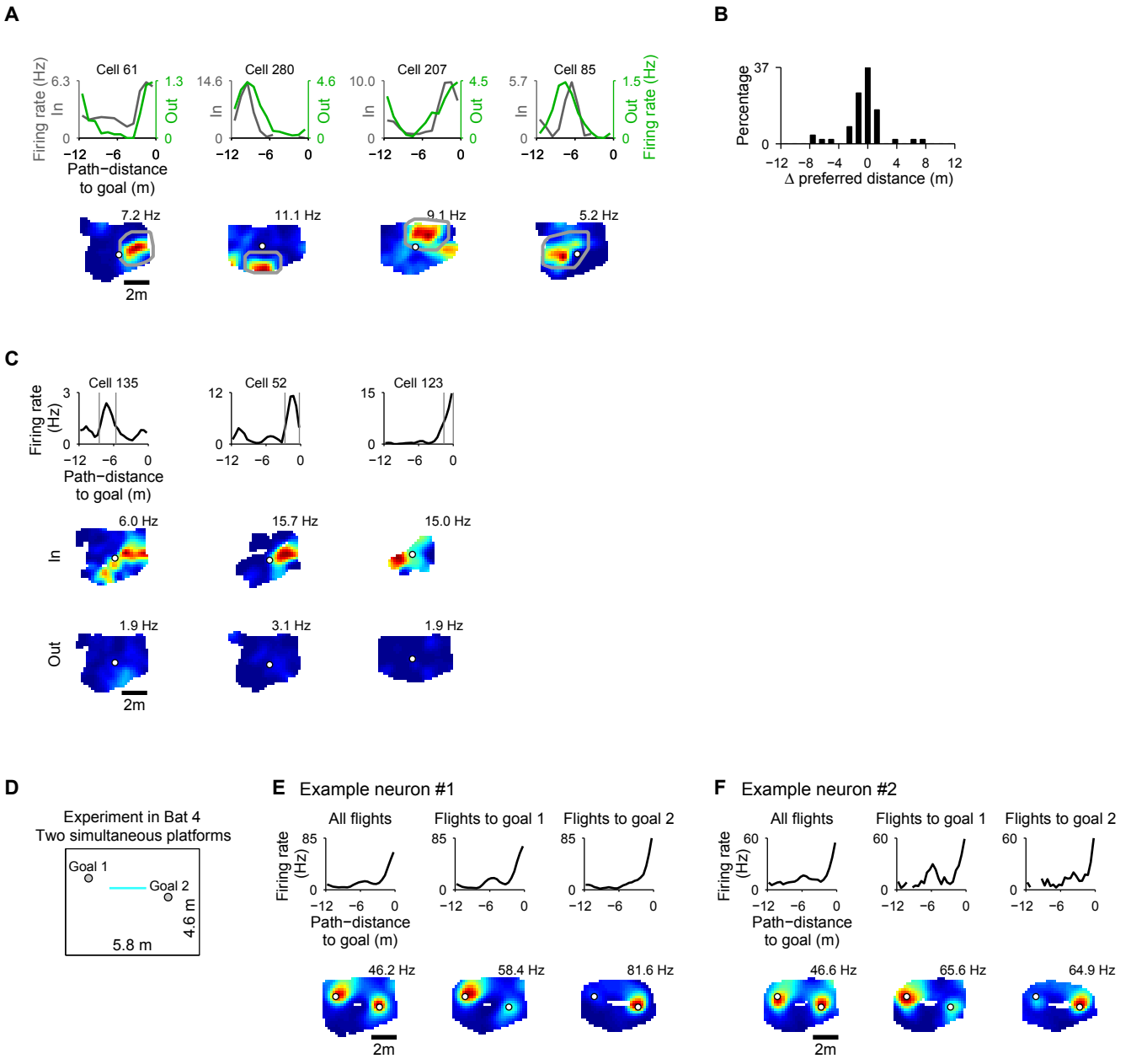

fig. S12. The path-distance tuning did not result from the place tuning. (**A**) Examples of four cells (columns) exhibiting similar path-distance tuning in and out of the place field. Top row: path-distance tuning curves computed from in-field spikes and behavioral data (grey curves) and out-of-field spikes and behavioral data (green curves). Bottom row: firing-rate map (top view); the thick gray line defines our 'in-field area'. (**B**) Distribution of the difference in preferred path-distance between in-field and out-of-field for all goal-distance cells. The small differences across the population (peak at ~0-meter difference) indicate that the path-distance signal is independent of the hippocampal place signal. (**C**) Examples of three cells (columns) that exhibit different place tuning in and out of the path-distance "field" (Methods). Top row: path-distance tuning. The 'in-field' is defined in-between the two grey vertical lines. Middle row: firing-rate maps based on the in-field spikes and in-field behavioral data. Bottom row: firing-rate maps based on the out-of-field spikes and out-of-field behavioral data. The colors of the firing-rate maps are normalized to the same maximum for each neuron. Note that the difference between the in/out maps (both in firing-rate and in field-location) suggests that the apparent place-tuning of these cells is in fact a result of their path-distance tuning. (**D-F**) We conducted a separate experiment in a 4th bat, in which we recorded 5 goal-distance cells (out of a total population of 34 recorded cells), in a task with *two simultaneous goals* – which allowed us to directly demonstrate that the distance tuning is genuine and independent of the place tuning. (**D**) Experimental setup for bat 4, with two elevated platforms as goals, 0.4×0.4 m in size, which were placed at the east and west sides of the flight-room (same room as for bats 1,2,3 – size: 5.8×4.6×2.7 m). The curtain in the middle of the room (light blue horizontal line) was transparent in this experiment (bat 4), but did not allow the bat to fly through. This setup was not part of the main analy-

Supplementary figure 12 - page 2

Continued from previous page

sis of the goal-direction cells (Fig. 1), due to the simultaneity of the two goals. (**E-F**) Two example cells. Upper row: path-distance tuning. Lower row: Firing-rate maps (top view). All the plots in panel E correspond to one cell, and all the plots in panel F correspond to a second cell. For each neuron, we separated the flights according to the landing platform: goal 1 versus goal 2. Left column: data for all flights. Middle column: data only for flights in which the bat landed on goal 1. Right column: data only for flights in which the bat landed on goal 2. Note that, for both neurons, the distance-tuning remained roughly the same, while the place-tuning changed substantially between flights to goal 1 versus flights to goal 2 – with the neuron firing maximally at a short path-distance from the current goal – suggesting that these neurons did *not* encode the absolute position of the animal, but rather encoded the path-distance to the goal on which the bat will land.

Supplementary figure 13

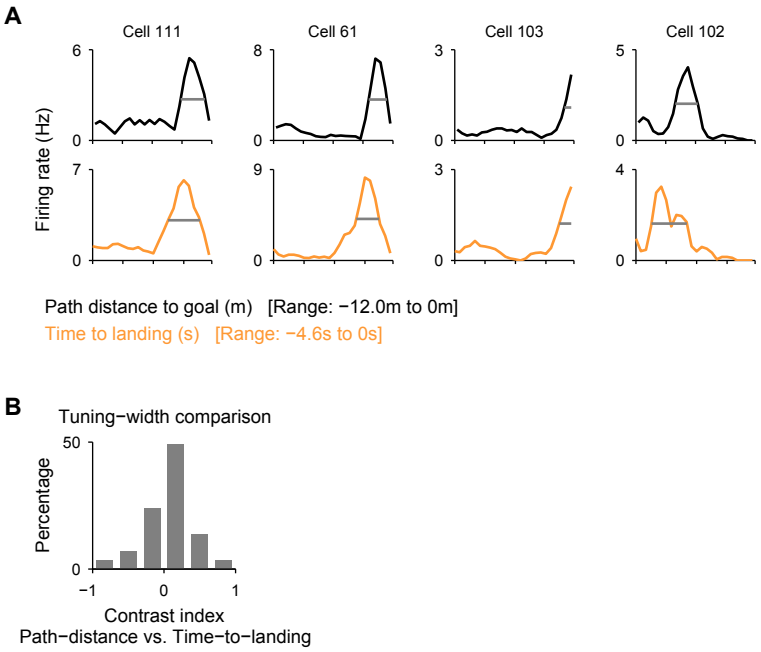

fig. S13. Cells were slightly better tuned to path-distance than to time-to-landing. Path-distance (distance-to-landing) and time-to-landing are two behaviorally-correlated variables; here we tested whether neurons were better tuned to one variable than to the other. (**A**) Examples of four cells encoding the path-distance to the goal with narrower tuning-width than the time-to-landing tuning width. Top: path-distance tuning curve (black) and tuning width at half-height (gray horizontal line). Bottom: time-to-landing tuning curve (orange) and tuning width at half-height (gray line). Both tuning curves were computed with the same number of bins (24 bins), and the range of times was defined by the range of the path-distance (12 m) divided by the average speed of the bats (2.6 m/s).
(**B**) Distribution of contrast-index between the time-to-landing tuning width and the path-distance tuning width:

(time width – (distance width/speed)) / (time width + (distance width/speed))

for all the cells tuned either to path-distance or to time-to-landing (n=59; we pooled here all neurons tuned to path-distance and all neurons tuned to time-to-landing; for the latter cells, we used similar inclusion criteria as for path-distance cells). Cells were slightly better tuned to the path-distance than to time-to-landing, indicated by the rightward shift in the histogram (sign-test: $P < 0.02$; t-test: $P = 0.19$).

Supplementary figure 14

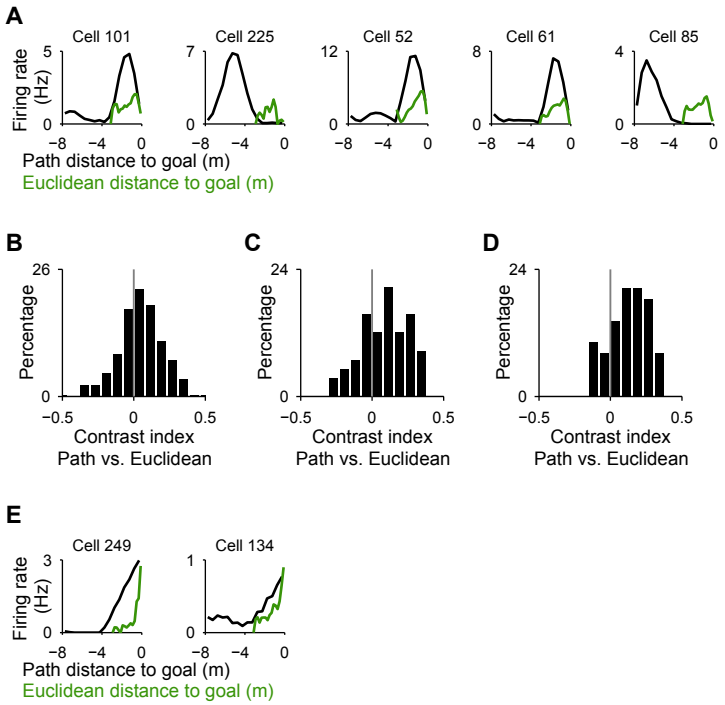

fig. S14. Cells were more tuned to the path-distance than to the Euclidean distance to the goal, although some cells encoded better the Euclidean distance. (**A**) Examples of five cells encoding the path-distance to the goal, but not the Euclidean-distance to the goal. The path-distance tuning (black) and the Euclidean-distance tuning (green) are both plotted with the same number of bins – demonstrating a sharper tuning to path-distance in these cells (black lines). (**B-D**) Distributions of contrast index between the path-distance index (*PDI*) and the Euclidean-distance index (*EDI*) (Methods): (*PDI* – *EDI*) / (*PDI* + *EDI*). All 3 distributions were significantly positively-shifted, indicated stronger tuning to path-distance than to the Euclidean-distance to the goal. (**B**) Distribution of the contrast-index for all the recorded cells (n = 309; t-test: $P < 10^{-6}$). (**C**) Distribution of the contrast-index for all the goal-direction cells that were significantly tuned to the central goal (n = 58; t-test: $P < 10^{-3}$). (**D**) Distribution of the contrast-index for all the significant goal-distance cells (n = 49; t-test: $P < 10^{-7}$). (**E**) Examples of two cells encoding the Euclidean-distance to the goal better than the path-distance to the goal. The path-distance tuning (black) and the Euclidean-distance tuning (green) are both plotted with the same number of bins – demonstrating a sharper tuning to Euclidean-distance in these 2 cells (green lines). Both of these cells had a negative contrast index, i.e., they were below 0 in the histogram in panel B – indicating better tuning to Euclidean distance.

References and Notes

1. J. O'Keefe, J. Dostrovsky, The hippocampus as a spatial map. Preliminary evidence from unit activity in the freely-moving rat. *Brain Res.* **34**, 171–175 (1971). doi:10.1016/0006-8993(71)90358-1 Medline

2. M. A. Wilson, B. L. McNaughton, Dynamics of the hippocampal ensemble code for space. *Science* **261**, 1055–1058 (1993). doi:10.1126/science.8351520 Medline

3. N. Ulanovsky, C. F. Moss, Hippocampal cellular and network activity in freely moving echolocating bats. *Nat. Neurosci.* **10**, 224–233 (2007). doi:10.1038/nn1829 Medline

4. T. Hafting, M. Fyhn, S. Molden, M.-B. Moser, E. I. Moser, Microstructure of a spatial map in the entorhinal cortex. *Nature* **436**, 801–806 (2005). doi:10.1038/nature03721 Medline

5. M. M. Yartsev, M. P. Witter, N. Ulanovsky, Grid cells without theta oscillations in the entorhinal cortex of bats. *Nature* **479**, 103–107 (2011). doi:10.1038/nature10583 Medline

6. J. S. Taube, R. U. Muller, J. B. Ranck Jr., Head-direction cells recorded from the postsubiculum in freely moving rats. I. Description and quantitative analysis. *J. Neurosci.* **10**, 420–435 (1990). Medline

7. A. Finkelstein, D. Derdikman, A. Rubin, J. N. Foerster, L. Las, N. Ulanovsky, Three-dimensional head-direction coding in the bat brain. *Nature* **517**, 159–164 (2015). doi:10.1038/nature14031 Medline

8. B. E. Pfeiffer, D. J. Foster, Hippocampal place-cell sequences depict future paths to remembered goals. *Nature* **497**, 74–79 (2013). doi:10.1038/nature12112 Medline

9. A. Johnson, A. D. Redish, Neural ensembles in CA3 transiently encode paths forward of the animal at a decision point. *J. Neurosci.* **27**, 12176–12189 (2007). doi:10.1523/JNEUROSCI.3761-07.2007 Medline

10. B. L. McNaughton, J. J. Knierim, M. A. Wilson, in *The Cognitive Neurosciences,* M. Gazzaniga, Ed. (MIT Press, 1995), pp. 585–595.

11. N. Burgess, J. O'Keefe, Neuronal computations underlying the firing of place cells and their role in navigation. *Hippocampus* **6**, 749–762 (1996). doi:10.1002/(SICI)1098-1063(1996)6:6<749:AID-HIPO16>3.0.CO;2-0 Medline

12. D. Bush, C. Barry, D. Manson, N. Burgess, Using grid cells for navigation. *Neuron* **87**, 507–520 (2015). doi:10.1016/j.neuron.2015.07.006 Medline

13. M. Stemmler, A. Mathis, A. V. Herz, Connecting multiple spatial scales to decode the population activity of grid cells. *Sci. Adv.* **1**, e1500816 (2015). doi:10.1126/science.1500816 Medline

14. M. Müller, R. Wehner, Path integration in desert ants, *Cataglyphis fortis*. *Proc. Natl. Acad. Sci. U.S.A.* **85**, 5287–5290 (1988). doi:10.1073/pnas.85.14.5287 Medline

15. A. S. Etienne, R. Maurer, J. Berlie, B. Reverdin, T. Rowe, J. Georgakopoulos, V. Séguinot, Navigation through vector addition. *Nature* **396**, 161–164 (1998). doi:10.1038/24151 Medline

16. H. G. Wallraff, *Avian Navigation: Pigeon Homing as a Paradigm* (Springer, 2005).

17. C. R. Gallistel, *The Organization of Learning* (MIT Press, 1990).

18. R. F. Wang, E. S. Spelke, Updating egocentric representations in human navigation. *Cognition* **77**, 215–250 (2000). doi:10.1016/S0010-0277(00)00105-0 Medline

19. P. Foo, W. H. Warren, A. Duchon, M. J. Tarr, Do humans integrate routes into a cognitive map? Map- versus landmark-based navigation of novel shortcuts. *J. Exp. Psychol. Learn. Mem. Cogn.* **31**, 195–215 (2005). doi:10.1037/0278-7393.31.2.195 Medline

20. Materials and methods are available as supplementary materials.

21. A. Rubin, M. M. Yartsev, N. Ulanovsky, Encoding of head direction by hippocampal place cells in bats. *J. Neurosci.* **34**, 1067–1080 (2014). doi:10.1523/JNEUROSCI.5393-12.2014 Medline

22. L. Acharya, Z. M. Aghajan, C. Vuong, J. J. Moore, M. R. Mehta, Causal influence of visual cues on hippocampal directional selectivity. *Cell* **164**, 197–207 (2016). doi:10.1016/j.cell.2015.12.015 Medline

23. H. Eichenbaum, N. J. Cohen, Can we reconcile the declarative memory and spatial navigation views on hippocampal function? *Neuron* **83**, 764–770 (2014). doi:10.1016/j.neuron.2014.07.032 Medline

24. H. Eichenbaum, Time cells in the hippocampus: A new dimension for mapping memories. *Nat. Rev. Neurosci.* **15**, 732–744 (2014). doi:10.1038/nrn3827 Medline

25. A. Tsoar, R. Nathan, Y. Bartan, A. Vyssotski, G. Dell'Omo, N. Ulanovsky, Large-scale navigational map in a mammal. *Proc. Natl. Acad. Sci. U.S.A.* **108**, E718–E724 (2011). doi:10.1073/pnas.1107365108 Medline

26. S. S. Deshmukh, J. J. Knierim, Influence of local objects on hippocampal representations: Landmark vectors and memory. *Hippocampus* **23**, 253–267 (2013). doi:10.1002/hipo.22101 Medline

27. P. Georges-François, E. T. Rolls, R. G. Robertson, Spatial view cells in the primate hippocampus: Allocentric view not head direction or eye position or place. *Cereb. Cortex* **9**, 197–212 (1999). doi:10.1093/cercor/9.3.197 Medline

28. A. A. Wilber, B. J. Clark, T. C. Forster, M. Tatsuno, B. L. McNaughton, Interaction of egocentric and world-centered reference frames in the rat posterior parietal cortex. *J. Neurosci.* **34**, 5431–5446 (2014). doi:10.1523/JNEUROSCI.0511-14.2014 Medline

29. L. R. Howard, A. H. Javadi, Y. Yu, R. D. Mill, L. C. Morrison, R. Knight, M. M. Loftus, L. Staskute, H. J. Spiers, The hippocampus and entorhinal cortex encode the path and Euclidean distances to goals during navigation. *Curr. Biol.* **24**, 1331–1340 (2014). doi:10.1016/j.cub.2014.05.001 Medline

30. R. G. Morris, P. Garrud, J. N. Rawlins, J. O'Keefe, Place navigation impaired in rats with hippocampal lesions. *Nature* **297**, 681–683 (1982). doi:10.1038/297681a0 Medline

31. A. Sarel, A. Finkelstein, L. Las, N. Ulanovsky, paper presented at the Annual Meeting of the Israel Society for Neuroscience, Eilat, Israel, 7 to 9 December 2014.

32. M. M. Yartsev, N. Ulanovsky, Representation of three-dimensional space in the hippocampus of flying bats. *Science* **340**, 367–372 (2013). doi:10.1126/science.1235338 Medline

33. A. Tuval, N. Ulanovsky, L. Las, T. Bdolah-Abram, Y. Shilo-Benjamini, paper presented at the 13th International Congress of the Federation of Laboratory Animal Science Associations, Brussels, Belgium, 13 to 16 June 2016.

34. E. J. Markus, C. A. Barnes, B. L. McNaughton, V. L. Gladden, W. E. Skaggs, Spatial information content and reliability of hippocampal CA1 neurons: Effects of visual input. *Hippocampus* **4**, 410–421 (1994). doi:10.1002/hipo.450040404 Medline